

# Generalized hydraulic geometry: Derivation based on a multiscaling formalism

Boyko Dodov and Efi Foufoula-Georgiou

St. Anthony Falls Laboratory, Department of Civil Engineering, and National Center for Earth-surface Dynamics, University of Minnesota Twin Cities, Minneapolis, Minnesota, USA

Received 21 February 2003; revised 2 March 2004; accepted 9 March 2004; published 18 June 2004.

[1] Relationships between channel characteristics (e.g., mean depth, water surface width, mean velocity) and discharge, known as hydraulic geometry (HG), have been extensively used by hydrologists and geomorphologists since the seminal work of *Leopold and Maddock* [1953]. On the basis of recent empirical evidence that the parameters of at-site HG depend systematically on the contributing area (scale) and that the parameters of downstream HG depend on the frequency of discharge, we propose a multiscaling formalism within which to model and interpret both at-site and downstream HG in a homogeneous region. In particular, we postulate and test multiscaling models for cross-sectional area and discharge and derive generalized HG relationships that explicitly account for scale-frequency dependence. The multiscaling formalism is tested in several basins in Oklahoma and Kansas for drainage areas ranging from 2 to 20,000 km<sup>2</sup> and shows good agreement with the data. To quantify the effects that scale dependence in HG has on the hydrologic response of a basin, a geomorphologic nonlinear cascade of reservoirs model has been used to compute attributes of a representative hydrologic response function for various levels of catchment-averaged effective rainfall and different basin orders. The numerical experiment shows substantial differences in hydrologic response when using classical versus generalized HG. Finally, a preliminary effort is reported to generalize even further the HG relationships such that they can account for deviations from a single power law (e.g., consideration of two different power laws in low- and high-flow regimes) through the introduction of a bivariate mixed multiscaling framework. *INDEX TERMS*: 1860 Hydrology: Runoff and streamflow; 1824 Hydrology: Geomorphology (1625); 1821 Hydrology: Floods; 3220 Mathematical Geophysics: Nonlinear dynamics; *KEYWORDS*: hydraulic geometry, hydrologic response, scaling

**Citation:** Dodov, B., and E. Foufoula-Georgiou (2004), Generalized hydraulic geometry: Derivation based on a multiscaling formalism, *Water Resour. Res.*, 40, W06302, doi:10.1029/2003WR002082.

## 1. Introduction

[2] The dependencies between channel properties and river flows have been observed for a long time, and empirically described by the notion of hydraulic geometry (HG). Hydraulic geometry was first introduced in the pioneering work of *Leopold and Maddock* [1953] and refers to the power laws relating the channel width  $W$ , mean depth  $D$ , and mean velocity  $V$  to discharge  $Q$ :  $W = aQ^b$ ,  $D = cQ^f$ ,  $V = kQ^m$ . (Hereafter the width  $W$ , mean depth  $D$ , mean velocity  $V$ , cross-sectional area  $C_A$  and discharge  $Q$  are referred to as HG factors). These relationships have been observed to hold either for different discharges at an individual cross section (hereafter called at-station HG), or for different downstream locations related through some characteristic discharge of constant frequency of exceedance (hereafter denoted as downstream HG). Figure 1 (reproduced from *Leopold and Maddock* [1953]) illustrates the idea for one HG factor, the velocity.

[3] For at-station HG, the single power law relationships are widely used although some deviations from a single

power law have been reported in the literature, either as a change in the exponent in the log-log plot of velocity and discharge with increasing discharge, or in general as loss of log-log linearity when discharge increases [e.g., *Richards*, 1976; *Wong and Laurenson*, 1984; *Bates*, 1990; *Pilgrim*, 1976]. In contrast, the log-log linearity in downstream HG has been supported by many empirical [*Carlston*, 1969; *Park*, 1977] and theoretical [*Parker*, 1979; *Huang et al.*, 2002] studies. Many empirical models [e.g., see *Rhoads*, 1991] consider the proportionality coefficient and the exponents of hydraulic geometry as functions of some specific discharge and the grain size of bed and/or bank material. Since both grain size and discharge generally depend on the contributing area (scale), it is clear that the magnitude of the power law exponents will also depend on the contributing area and frequency of occurrence of a specific discharge.

[4] Analytical derivation of scale-frequency-dependent HG based on first principles is not known to the best of authors knowledge, and this is probably because the at-station and downstream hydraulic geometries represent two different (although mutually dependent) processes, which “live” in different timescales. On the other hand, approaching HG from a statistical point of view seems fruitful, especially given that a rigorous mathematical-statistical

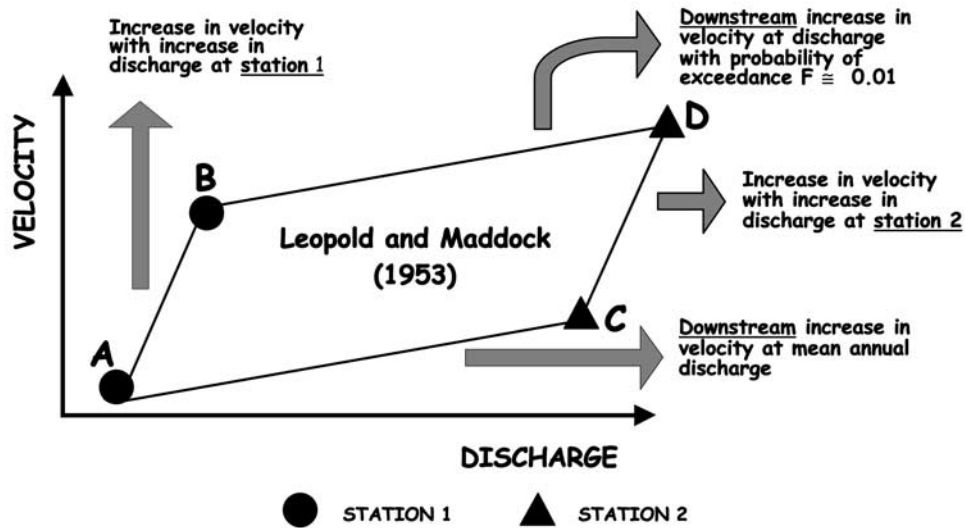


Figure 1. At-station and downstream HG [after Leopold and Maddock, 1953].

framework exists, that of “multiscaling scale invariance”, within which processes whose spatial variability changes with scale and frequency can be concisely described. In essence, multiscaling scale invariance implies that the probability distribution function of a random field indexed by scale, can be appropriately rescaled via a random or non-random function which depends on scale only. The multiscaling framework has been successfully employed to provide a theoretical basis for the empirically observed scale-dependent behavior of flood peaks in the context of regional quantile analysis [e.g., Gupta and Waymire, 1990; Gupta et al., 1994; Gupta and Dawdy, 1995]. Other applications of this concept have appeared in atmospheric turbulence, rain and clouds (e.g., see Schertzer and Lovejoy [1987] for an early reference), in river networks [e.g., Gupta and Waymire, 1989], and in solute transport [Sposito and Jury, 1988]. In this paper, it is shown that the multiscaling framework can provide a theoretical basis for interpreting and modeling the scale and frequency dependent relations between channel morphometry and discharge (known as HG).

[5] This paper is structured as follows. In section 2, empirical evidence is provided (based on 85 stations in Oklahoma and Kansas for basins ranging from 10 to above 10000 km<sup>2</sup>) that at-station HG depends systematically on scale and downstream HG depends on the frequency of the characteristic discharge. In section 3, a multiscaling model is proposed for channel cross-sectional area and discharge and is used to derive generalized at-station and downstream HG for cross-sectional area and velocity. The parameters of the generalized at-station HG are analytical functions of the multiscaling model parameters and the contributing area (scale). Analytical derivation of the parameters of the downstream HG is not possible and these have been computed numerically. The theoretically derived HG (both at-site and downstream) is compared to the empirical HG with good agreement, supporting thus the proposed generalized model. In section 4, the hydrologic response of a hypothetical catchment has been computed based on geomorphologic

nonlinear reservoirs in network model and assuming classical versus generalized HG. This comparison is revealing and highlights important implications of the scale-dependent (and thus spatially heterogeneous) HG on the nonlinearity of hydrologic response. Finally, based on the observation that a single power law relationship of velocity versus discharge may not hold for a wide range of discharges (it often breaks for discharges close and above bank-full), and also that there is a considerable spread in the log-log linear relationships of HG (pointing to the fact that they have to be seen as stochastic and not deterministic relationships), an extension of the lognormal multiscaling framework to a bivariate mixed lognormal multiscaling framework is proposed in section 5. A preliminary analysis shows indeed that this extended framework has the potential to capture the scale frequency dependence of HG for composite log-log linear relationships.

## 2. Empirical Evidence for the Need to Revisit Hydraulic Geometry

[6] We start with a brief review of the Leopold and Maddock's [1953] original work. The at-station HG relationships were proposed based on analysis of 20 natural river cross sections representing a large variety of rivers in the Great Plains and the Southwest. They found that the relations of width, mean depth and mean velocity to discharge (up to bank-full stage) were in the form of simple power laws:  $W = aQ^b$ ,  $D = cQ^f$  and  $V = kQ^m$ , with average values of the at-site exponents:  $b = 0.26$ ,  $f = 0.40$ , and  $m = 0.34$ . Some considerable variation in the exponents was reported, but no quantitative explanation of this variability was attempted since the effort was to capture the general trends. Besides, the stations used in the analysis had large contributing areas (2500 to 70,000 km<sup>2</sup>), thus neglecting the possibility of observing a trend in the at-station exponents at smaller scales.

[7] Regarding the downstream HG, extensive analysis of several rivers of different sized drainage basins and widely different physiographic settings indicated that the rates of increase in depth, width and velocity with increasing mean

annual discharges in the downstream direction were power laws with average values of exponents  $b = 0.5$ ,  $f = 0.40$  and  $m = 0.1$  [Leopold and Maddock, 1953]. However, the conclusion that the downstream HG exponents do not depend on the frequency of discharge was based on the analysis of data from two regions: Maumee and Scioto basins in Ohio and Yellowstone River basin in Wyoming for which discharges other than the mean annual discharge (namely discharges with frequency of exceedance  $F = 1, 4, 10, 30$  and 50% of time) were considered. Although the plots showed some variability in the log-log slopes for different frequencies, Leopold and Maddock considered the general trends and proposed that the exponents could be assumed constant. Again, the contributing areas of the chosen stations were of orders  $O(10^2 \text{ to } 10^5)$  neglecting a possible trend, which could be observed at smaller scales ( $10^0 \text{ to } 10^2 \text{ km}^2$ ). Referring to Figure 1, the Leopold and Maddock [1953] relationships imply parallel lines in the log-log space, i.e.,  $AC \parallel BD$  and  $AB \parallel CD$ , since the slopes are independent of contributing area and exceedance frequency of discharge.

[8] Similar results (in terms of constant exponents in the power law relationships) were obtained by Stall and Fok [1968] in their analysis of data from 18 basins in Illinois. Stall and Fok [1968] observed that in the interval of frequencies of exceedance  $F$  (the proportion of time in which a particular HG factor is greater than or equal to a given value) between 0.1 and 0.9, the logarithm of hydraulic geometry factors can be represented as linear functions of  $F$  and of the logarithm of contributing area  $A$  in the form:

$$\ln W(F, A) = \alpha'_W + \beta'_W F + \gamma'_W \ln A \quad (1a)$$

$$\ln C_A(F, A) = \alpha'_{C_A} + \beta'_{C_A} F + \gamma'_{C_A} \ln A \quad (1b)$$

$$\ln V(F, A) = \alpha'_V + \beta'_V F + \gamma'_V \ln A \quad (1c)$$

$$\ln D(F, A) = \alpha'_D + \beta'_D F + \gamma'_D \ln A \quad (1d)$$

$$\ln Q(F, A) = \alpha'_Q + \beta'_Q F + \gamma'_Q \ln A \quad (1e)$$

where  $\alpha'_{(\cdot)}$ ,  $\beta'_{(\cdot)}$  and  $\gamma'_{(\cdot)}$  are empirical regression coefficients and  $C_A$  denotes cross-sectional area. Combining equations (1a) to (1d) with equation (1e) it can be shown that the above equations are consistent with Leopold and Maddock's [1953] power laws with exponents constant at-station and downstream. If plotted as logarithms of HG factors versus logarithm of contributing area for different frequencies, the above equations represent parallel straight lines with slopes  $\gamma'_{(\cdot)}$  and intercepts  $\alpha'_{(\cdot)} + \beta'_{(\cdot)} F$ .

[9] Considering the results of Stall and Fok [1968], one has to take into account the fact that the measurements of HG factors at flows close to bank-full ones are strongly influenced by dynamic storages due to backwater effects, increase in the content of suspended sediment, increase of the momentum transfer toward banks, secondary currents, etc. Taking into account the fact that on the mean the channel profile diverges faster downstream than upstream, it is expected that in the downstream direction the effect of the dynamic storage will increase faster with discharge, resulting in a lower rate of increase of velocity and higher rate of increase in depth and cross-sectional area. In contrast, the

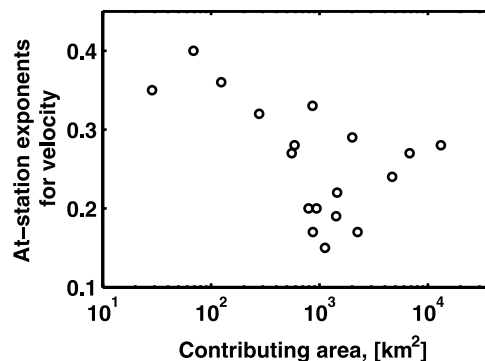


**Figure 2.** Plot of at-station exponents for velocity for 18 stations in Sangamon River basin, Illinois (reproduced from the values of Table 8 of Stall and Fok [1968]).

upstream rate of increase of velocity will be higher, and the rate of increase of the cross-sectional area and depth will be lower. The closer the flow conditions to bank-full ones, the stronger the effect of dynamic storage downstream. As a result, the mean velocity at bank-full flow will become almost constant at any cross section, while for lower discharges the mean velocity will increase with contributing area. In the context of the Stall and Fok's [1968] relationships such a scenario will imply nonconstancy of the parameters  $\gamma'_{(\cdot)}$  in terms of different slopes for different frequencies in equation (1) equation (1). If for example we assume that  $\gamma'_{(\cdot)}$  are linearly dependent on frequency, it can be shown that the exponents of the at-station relationships are functions of the contributing area and the downstream exponents, functions of the frequency. As will become apparent later, the assumption of linear dependency of  $\gamma'_{(\cdot)}$  on frequency of exceedance is a special case of the proposed multiscaling framework for frequencies between 0.1 and 0.9. Careful examination of Stall and Fok's [1968] observations actually supports the above considerations: the results published in their paper for Sangamon River basin undoubtedly show dependence of the at-station exponents on scale (see Figure 2 reproduced from their tabulated results), although this was not explicitly considered in their analysis.

[10] To examine independently the assumption about the constancy of the exponents for a larger number of stations and in a region with relatively homogeneous topographic, geologic and climatic conditions we analyzed data from 85 gauging stations from Oklahoma and Kansas, USA (see Figure 3). The data consists of (1) independent measurements of width, mean depth, cross-sectional area, mean velocity and discharge under different flow conditions (up to several hundred measurements per station) and (2) time series of at least 5 years of daily discharges for every station. Gages were chosen such that there are only minor streamflow regulations upstream and such that there is a similar underlying geology of drainage basins in order to avoid significant effects of geologic controls on the analysis.

[11] It is noted that for most of the stations, good log-log linearity between hydraulic geometry factors was observed. Figure 4 shows a typical example of these log-log relationships. Note that the  $(C_A, Q)$  relationship shows the best log-log linearity, while a lot of scatter is found in the  $(V, Q)$  plots and, in general, deviation from log-log linearity is observed

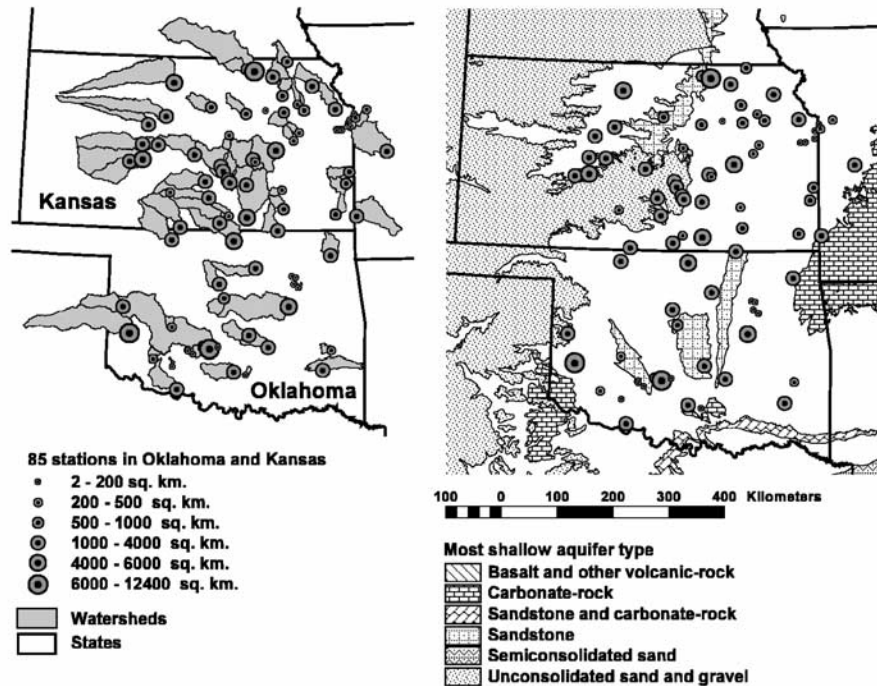


**Figure 3.** (left) Locations of the 85 stations used in our analysis with their corresponding watersheds and (right) type of most shallow aquifers. The ID numbers of the stations and their contributing areas are given in Table 1.

in the  $(W, Q)$  and  $(D, Q)$  relationships, especially for high and low discharges. Table 1 lists the fitted exponents and preexponents of the  $(C_A, Q)$  and  $(V, Q)$  power law relationships for all 85 stations used in the analysis.

[12] Table 2 shows the overall goodness of fit of these log-log relationships in terms of the mean  $R^2$  for all 85 stations. Table 2 also includes measures of the linear correlations between the residuals in terms of mean run test scores and the average (over the 85 stations) of the means of the first 10 autocorrelation coefficients. The best candidate for a good log-log linear relationship is the cross-sectional area (for detailed discussion on the at-station statistical properties of HG factors, see *Dodov* [2003]). The mean  $R^2$  for the velocity is low but the residuals are uncorrelated, which suggests that power laws are representative but with a lot of scatter. The relationships for the width and the depth show lower mean  $R^2$  but more correlated residuals and their log-log linearity is, in general, questionable. The strong power law relationships between cross-sectional area and discharge motivated us to consider  $C_A$  as the channel morphometry parameter for the multiscaling framework proposed in the next section.

[13] Figure 5 shows the fitted at-station HG for  $C_A$  and  $V$  for two stations (of areas approximately 20 and 4000 km<sup>2</sup>, respectively) and the discharge frequency curve constructed from daily flows. As can be seen, the slopes of the log-log linear relationships depend on the contributing area. In Figure 6 we plot the at-station exponents for cross-sectional area and velocity (estimated from the above fitted log-log relationships to each of the 85 stations) versus contributing area, and in Figure 7 we plot the downstream HG for  $C_A$  and  $V$  for discharge frequencies of exceedance 90 and 1%. (The

Weibull plotting position was used to estimate nonparametrically discharges of a specific frequency.) Obviously there is a trend of the at-station exponents with contributing area (Figure 6) and a dependence of the downstream exponents on the frequency of discharge (Figure 7). These trends present the motivation of our work to revisit HG and propose a generalized model capable of reproducing in a parsimonious way the scale and frequency dependence of HG.

[14] In the next section, we (1) propose a class of multiscaling models for HG factors  $C_A$  and  $Q$ , (2) fit these multiscaling models to observations and test their validity, and (3) derive the exponents of the at-station and downstream HG for  $C_A$  and  $V$  in terms of the parameters of the multiscaling models. Before proceeding to the next section the reader is advised to read Appendix A for a brief review of the multiscaling framework or refer to the original work of *Gupta and Waymire* [1990] and *Gupta et al.* [1994] for an in-depth presentation of multiscaling in the context of flood peak analysis.

### 3. A Multiscaling Formalism of Hydraulic Geometry

#### 3.1. Multiscaling of Discharge and Cross-Sectional Area

[15] The following hypothesis is posed: The discharge and cross-sectional area obey log-Lévy multiscaling models with  $p$ th quantiles in the form:

$$\ln C_{A_p}(A) = (\alpha_{C_A} + \beta_{C_A} \ln A) + (\gamma_{C_A} + \delta_{C_A} \ln A)^{1/\alpha_{C_A}} w_p, \quad (2a)$$

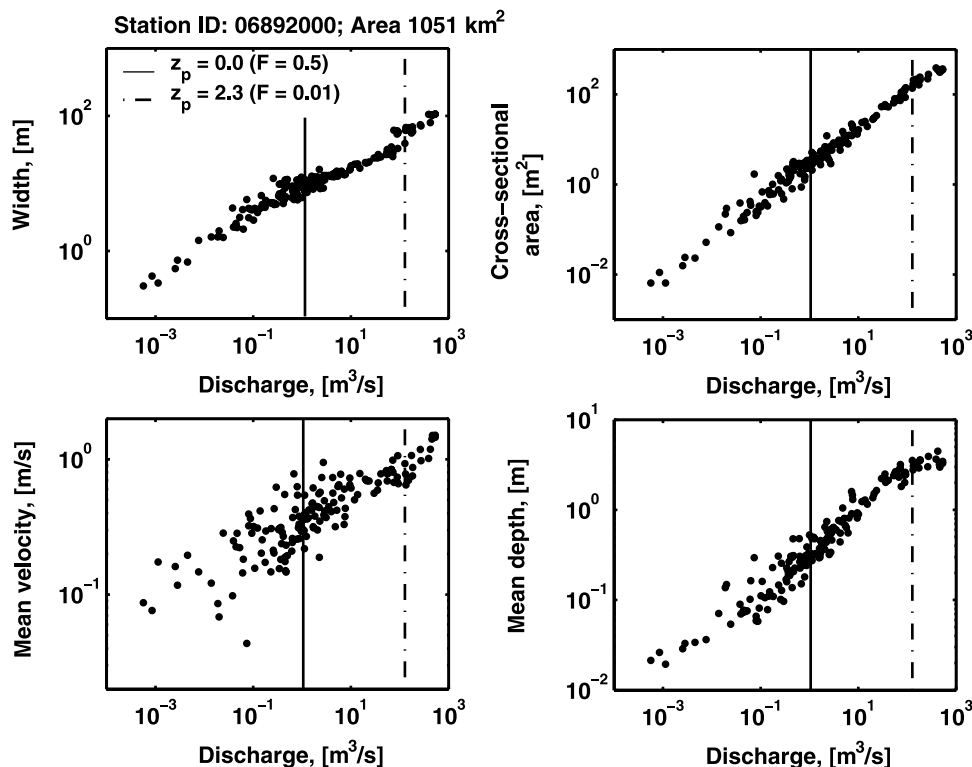


**Figure 4.** Example log-log relationships between width, cross-sectional area, mean velocity, mean depth, and discharge.

$$\ln Q_p(A) = (\alpha_Q + \beta_Q \ln A) + (\gamma_Q + \delta_Q \ln A)^{1/\alpha_{w_p}},$$

$$\text{for } A_l^0 < A < A_l^1 \quad (2b)$$

where  $\alpha'_{(\cdot)}$ ,  $\beta'_{(\cdot)}$ ,  $\gamma'_{(\cdot)}$  and  $\delta'_{(\cdot)}$  are parameters,  $w_p$  denotes the  $p$ th quantile of  $-W$ , where  $W$  has a Lévy stable density with characteristic exponent  $\alpha$ ,  $A$  is the contributing area, and  $A_l^0$  and  $A_l^1$  represent some limiting contributing areas within which the scaling behavior holds (see background in Appendix A).

[16] The general multiscaling framework of *Gupta and Waymire* [1990] can accommodate a wide class of log-Lévy stable distributions for the quantities of interest. Lévy stable distributions are, in general, four parameter distributions with probability density  $S(x; \alpha, \beta, \delta, c)$  where  $0 < \alpha \leq 2$  is a characteristic exponent,  $-1 < \beta \leq 1$  is a skewness or symmetry parameter,  $-\infty < \delta < \infty$  is a location parameter, and  $c > 0$  is a scale parameter. In the symmetric case ( $\beta = 0$ ), this class includes the Cauchy ( $\alpha = 1$ ) and Gaussian,  $N(\alpha = 2, \beta = \mu, 2c^2 = \sigma^2)$  distributions. The characteristic function of the symmetric stable class [*Lamperti*, 1966] is

$$\rho(\xi)|_{\beta=0} = e^{i\delta\xi - |\xi|^\alpha} = \cos(\delta\xi)e^{-|\xi|^\alpha} + i \sin(\delta\xi)e^{-|\xi|^\alpha}$$

$$= C(\xi) + iS(\xi) \quad (3)$$

where  $\xi$  is a real number in  $(0, \pi/2]$ .

[17] *Gupta et al.* [1994] attempted estimation of log-Lévy multiscaling models for maximum annual floods. Since overall estimation of the parameter  $\alpha$  proved difficult, the special models of ( $\beta = 0, \alpha = 2$ ;  $\beta = 0, \alpha = 1.5$ ;  $\beta = 0, \alpha = 1$  and  $\beta \pm 1, \alpha = 1.5$ ) were fitted and the lognormal model ( $\beta = 0, \alpha = 2$ ) ended up being selected as their working model. Yet, significant deviations from the lognormal distribution were reported as it is known that maximal annual floods

have in general thicker tails than lognormal models and extreme type distributions have been the choice for floods. In contrast, lognormal distributions have generally offered good approximations for the daily discharges we consider here and have been used extensively for flow duration curves [e.g., see *Ashmore and Day*, 1988; *LeBoutillier and Waylen*, 1993]. Examination of the empirical probability distributions of  $C_A$  and  $Q$  showed that these distributions are well approximated as symmetric in the log domain. Therefore the assumption of  $\beta = 0$  was made and symmetric stable laws were fitted to daily discharges for the 85 analyzed stations using the method developed by *Arad* [1980]. This method is based on a linear regression of  $\log[-\log \hat{C}(\xi)]$  on  $\log|\xi|$  where  $\hat{C}(\xi)$  is the sample characteristic function (recall that because of the symmetry the characteristic function is real, i.e.,  $S(\xi) = 0$ ). If the data obey a symmetric Lévy stable distribution, the plot should form a straight line with slope  $\alpha$  and intercept  $\log(c^\alpha)$ . Figure 8 shows an example of these plots for daily  $Q$  and for two stations of different drainage area, approximately 20 and 8000 km<sup>2</sup>, respectively. Fitting each of these plots with a single straight line (overall, not a bad approximation) resulted in estimates of the characteristic exponent  $\alpha$  as shown in Figure 9. Deviation of  $\alpha$  from the value of 2 implies deviation from a lognormal distribution, which might be the case especially for larger areas as suggested by Figure 9.

[18] It is noted that the multiscaling model of equation (2) implicitly assumes the existence of a single log-Lévy distribution (single value of  $\alpha$ ) that represents well the PDFs at all scales. In fact, the value of  $\alpha$  in equation (2) would be estimated by fitting (as explained in the next section) all the parameters of the multiscaling models (2a)

**Table 1.** List of the 85 Stations Used in the Analysis Together With Their Contributing Areas and the Parameters of the Fitted At-Station Power Laws for  $C_A$  and  $V$

Station ID	Contributing Area, km <sup>2</sup>	Cross-Sectional Area		Mean Velocity	
		Exponent $r$	Preexponent $q$	Exponent $m$	Preexponent $k$
73274408	2.85	0.60	1.20	0.40	0.83
73274406	8.91	0.74	1.50	0.26	0.67
6879650	10.59	0.66	1.96	0.34	0.51
7165565	14.11	0.79	2.78	0.21	0.36
7328180	18.98	0.61	1.63	0.39	0.61
7177800	19.49	0.70	2.96	0.30	0.34
7177650	21.23	0.60	2.29	0.40	0.44
6914990	22.81	0.78	2.33	0.22	0.43
7327442	30.03	0.67	1.69	0.33	0.59
7164600	31.58	0.64	2.38	0.36	0.42
6893560	38.55	0.55	4.02	0.45	0.25
7165562	46.08	0.78	3.38	0.22	0.30
7311200	63.69	0.74	3.01	0.26	0.33
6893300	68.86	0.70	2.70	0.30	0.37
6914950	74.30	0.67	2.56	0.33	0.39
7329852	114.17	0.82	2.93	0.18	0.34
6893080	119.09	0.69	3.16	0.31	0.32
7327447	160.25	0.64	2.35	0.36	0.43
7180500	284.78	0.66	2.63	0.34	0.38
6911900	295.13	0.84	2.39	0.16	0.42
7144910	302.90	0.86	2.34	0.14	0.43
6870300	310.67	0.85	3.58	0.15	0.28
7247500	315.84	0.74	1.96	0.26	0.51
7167500	333.97	0.87	2.04	0.13	0.49
7305500	341.73	0.84	2.38	0.16	0.42
7325800	341.73	0.80	2.36	0.20	0.42
7145700	398.69	0.82	3.17	0.18	0.32
6889200	406.45	0.82	2.43	0.18	0.41
6910800	458.23	0.80	2.63	0.20	0.38
6894000	476.35	0.75	2.28	0.25	0.44
6893500	486.71	0.82	1.64	0.18	0.61
7184000	510.01	0.85	3.43	0.15	0.29
7169800	569.55	0.82	2.94	0.18	0.34
7327550	610.98	0.59	3.61	0.41	0.28
6888000	629.10	0.65	3.51	0.35	0.28
6814000	714.53	0.83	2.59	0.17	0.39
6889500	750.78	0.71	3.69	0.29	0.27
6917380	755.95	0.81	2.61	0.19	0.38
6917000	763.72	0.81	3.68	0.19	0.27
6878000	776.66	0.82	3.88	0.18	0.26
6888500	818.09	0.72	3.33	0.28	0.30
7159750	828.44	0.84	2.54	0.16	0.39
6884200	890.58	0.83	2.25	0.17	0.44
6876700	994.13	0.75	4.57	0.25	0.22
6892000	1051.09	0.82	2.76	0.18	0.36
6885500	1061.44	0.87	2.80	0.13	0.36
7160500	1061.44	0.83	2.99	0.17	0.33
7147070	1102.86	0.83	2.73	0.17	0.37
6890100	1115.81	0.81	2.69	0.19	0.37
7172000	1152.05	0.79	3.24	0.21	0.31
7191000	1165.00	0.79	2.63	0.21	0.38
7230500	1180.53	0.73	3.00	0.27	0.33
7153000	1491.20	0.78	2.48	0.22	0.40
6863500	1537.80	0.86	2.66	0.14	0.38
7329700	1563.68	0.64	3.60	0.36	0.28
7311500	1597.34	0.89	2.33	0.11	0.43
7145200	1682.77	0.79	3.30	0.21	0.30
7335790	1832.93	0.86	2.92	0.14	0.34
7143300	1884.71	0.88	3.46	0.12	0.29
7141175	1902.83	0.87	2.93	0.13	0.34
7143665	1905.42	0.90	3.04	0.10	0.33
7180400	1952.02	0.86	2.05	0.14	0.49
7143672	1964.96	0.95	2.57	0.05	0.39
7144780	2037.45	0.77	3.35	0.23	0.30
7151500	2055.57	0.76	3.05	0.24	0.33
7316500	2055.57	0.82	2.42	0.18	0.41
7231000	2239.38	0.78	2.27	0.22	0.44
7149000	2337.76	0.76	2.96	0.24	0.34
7148400	2612.18	0.85	2.43	0.15	0.41
7186000	3013.46	0.65	3.66	0.35	0.27

Table 1. (continued)

Station ID	Contributing Area, km <sup>2</sup>	Cross-Sectional Area		Mean Velocity	
		Exponent <i>r</i>	Preexponent <i>q</i>	Exponent <i>m</i>	Preexponent <i>k</i>
7141780	3085.95	0.97	2.72	0.03	0.37
7144100	3207.62	0.90	2.40	0.10	0.42
6921760	3287.88	0.84	4.21	0.16	0.24
7144200	3435.45	0.92	2.16	0.08	0.46
7141900	3650.32	0.83	3.64	0.17	0.27
6867000	3888.50	0.83	2.26	0.17	0.44
7182250	4504.65	0.90	2.45	0.10	0.41
7152000	4812.73	0.90	1.69	0.10	0.59
7147800	4867.10	0.74	3.87	0.26	0.26
7243500	5224.36	0.98	1.53	0.02	0.65
7141200	5560.92	0.91	3.10	0.09	0.32
6872500	5993.26	0.88	2.43	0.12	0.41
7301500	6050.21	0.78	3.13	0.22	0.32
6884400	8605.44	0.82	2.39	0.18	0.42
7328100	12392.97	0.73	3.49	0.27	0.29
Average parameters		0.79	2.77	0.21	0.38

and (2b) simultaneously. This value, admittedly different than the average value of  $\alpha$  obtained from Figure 9 ( $\bar{\alpha} = 1.92$ ), would certainly be very close to 2, thus making it appealing to adopt the lognormal multiscaling model (which offers easier fitting as well as interpretation) as a working model. Future investigation of the possible dependence of  $\alpha$  on scale would be interesting, however.

[19] It is important to notice at this point, that if two lognormally distributed random variables are related through a power law  $Y = aX^b$  (or  $\ln Y = \ln a + b \ln X$ ) it follows that their quantiles match, i.e.,

$$z_p^{\ln Y} = \frac{\ln Y - E[\ln Y]}{\{\text{Var}[\ln Y]\}^{1/2}} = \frac{b \ln X + \ln a - bE[\ln X] - \ln a}{\{b^2 \text{Var}[\ln X]\}^{1/2}} = \frac{b\{\ln X - E[\ln X]\}}{b\{\text{Var}[\ln X]\}^{1/2}} = \frac{\ln X - E[\ln X]}{\{\text{Var}[\ln X]\}^{1/2}} = z_p^{\ln X} \quad (4)$$

[20] Therefore, if  $Q$  and  $C_A$  obey the lognormal multiscaling models of equation (2) (with  $\alpha = 2$  and  $w_p = z_p$ , the  $p$ th standard normal quantile) then, in view of equation (4), the quantiles of  $V$  can be expressed through the ones of  $Q$  and  $C_A$  in the form

$$\ln V_p(A) = [\alpha_Q - \alpha_{C_A} + (\beta_Q - \beta_{C_A}) \ln A] + \left[ (\gamma_Q + \delta_Q \ln A)^{1/2} - (\gamma_{C_A} + \delta_{C_A} \ln A)^{1/2} \right] z_p \quad (5a)$$

It is noted that equation (5a) cannot be directly brought into a form required for multiscaling of  $V$ , i.e.,

$$\ln V_p(A) = (\alpha_V \pm \beta_V \ln A) + (\gamma_V \pm \delta_V \ln A)^{1/2} z_p, \quad (5b)$$

where  $\alpha_V$ ,  $\beta_V$ ,  $\gamma_V$  and  $\delta_V$  are explicit functions of  $\alpha_{(\cdot)}$ ,  $\beta_{(\cdot)}$ ,  $\gamma_{(\cdot)}$  and  $\delta_{(\cdot)}$  and  $(\cdot)$  denotes  $C_A$  and  $Q$ . In other words, if multiscaling lognormal models for  $Q$  and  $C_A$  exist, then the derived model for velocity is not itself multiscaling. Note that this does not imply that a multiscaling model would not be a good model for velocity if it were applied (i.e., fitted) directly to velocity observations. In fact, our results

(discussed in more detail in the next section) indicate that such a model would offer a good approximation apart from the fact that velocity observations seem to have a lot of scatter (see also the scatter in the  $(V, Q)$  relationships in Figures 4 and 5) increasing thus the uncertainty of parameter estimation in equation (5b).

[21] In section 3.2 we fit the lognormal multiscaling model to  $Q$  and  $C_A$  and test its validity. In addition, as an independent test of the validity of our hypothesis, we compare the derived statistical properties of  $V$ , i.e., computed via equation (5a), with the corresponding quantities estimated directly from the velocity observations.

### 3.2. Model Fitting and Hypothesis Testing

[22] A problem that arises with instantaneous observations is the fact that these observations do not usually sample the full probability space of the variables of interest and might not provide a good approximation of their true PDFs. For this, it was decided to use long records of daily discharges to obtain a representative PDF of instantaneous  $Q$  and to derive the PDFs of  $V$  and  $C_A$  from their power law relationships with  $Q$  at each individual station. This problem is schematically illustrated in Figure 10. For all the analysis that follows, quantities from the fitted (to daily discharges) PDFs of  $Q$ , and the derived PDFs for  $V$  and  $C_A$  were used.

Table 2. Goodness of Fit Tests of the At-Station HG Relationships Measured in Terms of Mean  $R^2$ , Run Test Score, and Autocorrelation Between the Residuals

HG Factor $\Lambda$	Average $R^2$ in $\ln \Lambda = f(\ln Q)$ at a Station	Analysis of Residuals	
		Average Run Test Statistics	Average Over the Mean of First 10 AC Coefficients
$W$	0.756	0.100	0.136
$C_A$	0.916	0.169	0.082
$V$	0.637	0.162	0.091
$D$	0.812	0.132	0.109

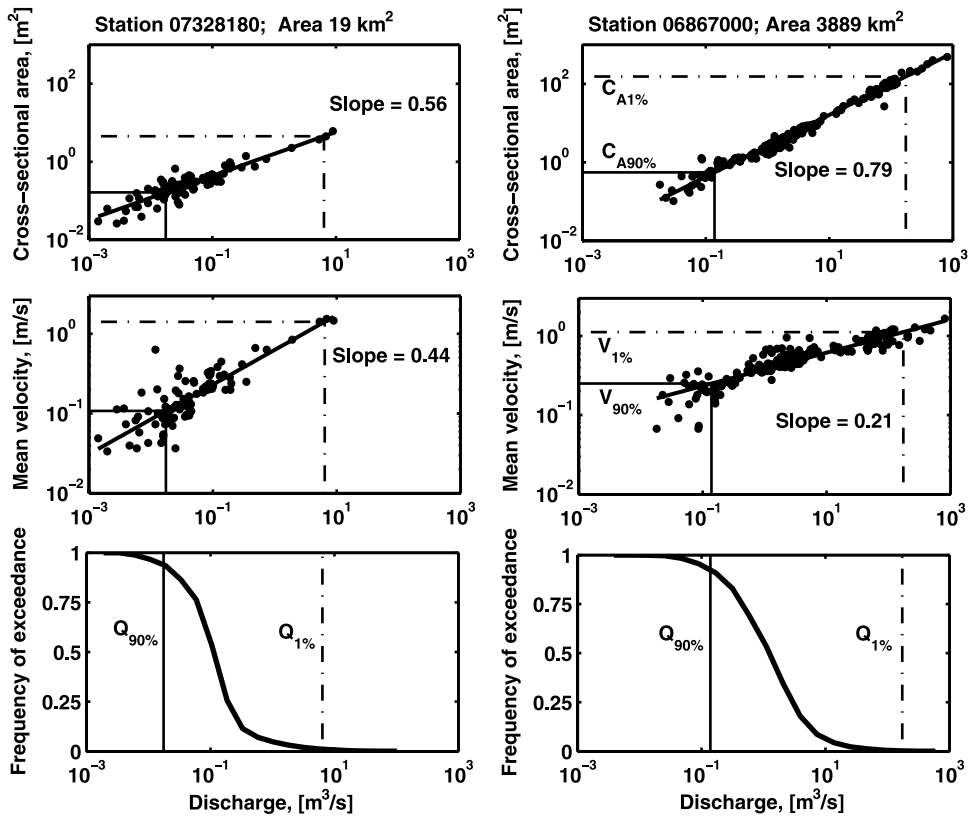


**Figure 5.** Example plots of at-station HG for cross-sectional area and velocity for two stations with areas of approximately 20 and 4000 km<sup>2</sup>. The bottom graphs show the empirical frequency of exceedance plots of daily discharge (flow duration curves) for these two stations.

The analysis was also done with hourly discharges, for all stations for which hourly data were available, but no significant differences were observed justifying the use of the readily available daily flows.

[23] In order to proceed with the testing of our hypothesis we need to estimate the eight parameters of the lognormal multiscaling models. This estimation is not trivial and is explained in detail below. Overall, a nonlinear optimization procedure is performed in two steps.

[24] 1. Considered at a station, equation (2) (now with  $\alpha = 2$  and  $w_p = z_p$  the  $p$ th standard normal quantile) represents linear relationships in the form

$$\ln Q_p(A_j) = h_Q(A_j) + m_Q(A_j)z_p \tag{6a}$$

$$\ln C_{A_p}(A_j) = h_{C_A}(A_j) + m_{C_A}(A_j)z_p \tag{6b}$$

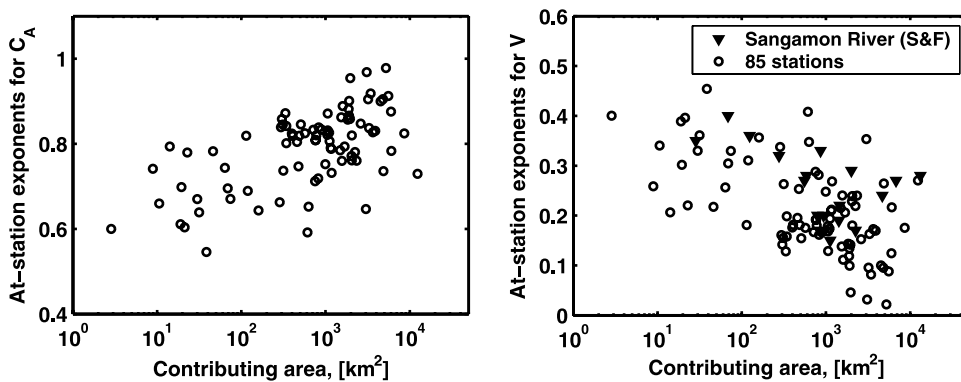


**Figure 6.** Plots of (left) at-station exponents for cross-sectional area and (right) velocity for the 85 stations in Oklahoma and Kansas versus contributing area. In the velocity plot we have superimposed the data from Table 8 of *Stall and Fok* [1968] for the Sangamon River, Illinois.

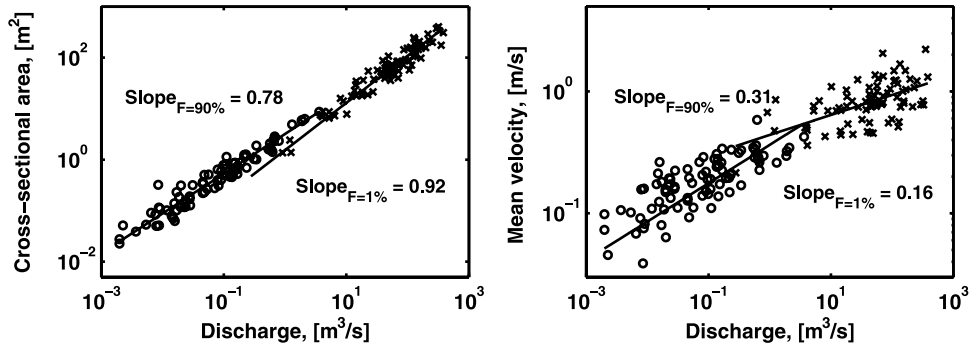


**Figure 7.** Downstream hydraulic geometry for cross-sectional area and velocity for two frequencies of exceedance  $F = 90\%$  and  $F = 1\%$  of discharge. Note that the slopes representing the downstream HG exponents are different for different frequencies of discharge.

where  $A_j$  is the contributing area of the  $j$ th station and  $h_{(.)}$  and  $m_{(.)}$  are parameters.

[25] Since  $A_j$  is a fixed value for any particular station, the above relationships have constant parameters  $h_{(.)}$  and  $m_{(.)}$  for each station. These parameters can be estimated independently for each station based on the available measurements of  $Q$  and  $C_A$  (in fact, based on the lognormality assumption,  $h_{(.)}$  would be the mean and  $m_{(.)}$  the standard deviation of the normal distributions fitted to the logs of the data). However, due to the sampling problem discussed above, only the quantiles of  $Q$  were estimated directly from observations (using records of at least 5 years of daily streamflows). Then, the corresponding quantiles of  $C_A$  were derived from the at-station HG between  $C_A$  and  $Q$  fitted to each station and the fitted PDF of  $Q$ .

[26] 2. The parameters of the lognormal multiscaling models of  $C_A$  and  $Q$  (both denoted below as  $\Lambda$ ) are estimated, by minimizing the sum of squares of the differences between the log of the empirical quantiles  $y_p^\Lambda(A_j)$ , estimated from step 1, and the theoretical quantiles  $\Lambda_p(\alpha_\Lambda, \beta_\Lambda, \gamma_\Lambda, \delta_\Lambda, A_j)$  defined by equation (2):

$$ss = \min_{(\alpha_\Lambda, \beta_\Lambda, \gamma_\Lambda, \delta_\Lambda)} \sum_j \sum_p \left[ \ln y_p^\Lambda(A_j) - \ln \Lambda_p(\alpha_\Lambda, \beta_\Lambda, \gamma_\Lambda, \delta_\Lambda, A_j) \right]^2 \tag{7}$$

for 10 different values of  $p$  (0.006, 0.026, 0.082, 0.202, 0.391, 0.609, 0.798, 0.918, 0.974 and 0.994). The idea behind this optimization technique is to fit the whole surface representing the PDFs of the two HG factors at all scales instead of fitting only their means and variances. A Nelder-

Mead simplex method was used for the minimization procedure. The estimated values of the lognormal multiscaling model parameters are given in Table 3.

[27] Our first step in the verification of the proposed lognormal models is similar to the methodology suggested by *Gupta et al.* [1994]. In Figure 11 we plot the values of  $h(A_j)$  and  $m(A_j)$  computed from the lognormal multiscaling models (as  $h(A_j) = \alpha_\Lambda + \beta_\Lambda \ln A_j$  and  $m(A_j) = (\gamma_\Lambda + \delta_\Lambda \ln A_j)^{1/2}$ ) for  $\Lambda = Q, C_A$ , and derived for  $V$  as  $h_V(A_j) = h_Q(A_j) - h_{C_A}(A_j)$  and  $m_V(A_j) = m_Q(A_j) - m_{C_A}(A_j)$  and compare them to the at-station empirical values. The agreement between the empirical and theoretical values is good with more scatter in the slopes  $m(A_j)$  (i.e., the standard deviations of logs of at-station  $Q, C_A$  and  $V$ ).

[28] To visually examine the goodness of fit of our model, we use the relationships obtained at step 1 above to calculate the  $p$ th quantiles  $Q_p^j, C_{A_p}^j$  and  $V_p^j$ , at each station  $j$  of area  $A_j$  for three different frequencies corresponding to  $z_p = 0, 1.5$  and  $2.9$  (it is noted that these frequencies were not among the 10 frequencies used for fitting the parameters). In Figure 12 we plot these quantities versus the logarithm of the contributing area  $A_j$  and compare them with the theoretical curves computed from the corresponding lognormal models for  $Q, C_A$  and derived for  $V$  for these three frequencies (i.e., equations 2a, b and 5a, respectively). The scatter is a bit higher for velocity, while for cross-sectional area and discharge the agreement between the model and the data is very good. Although the change of slope from one frequency to another is not drastic, it is noted that assuming constant slopes would imply constant exponents in the at-station HG (resulting

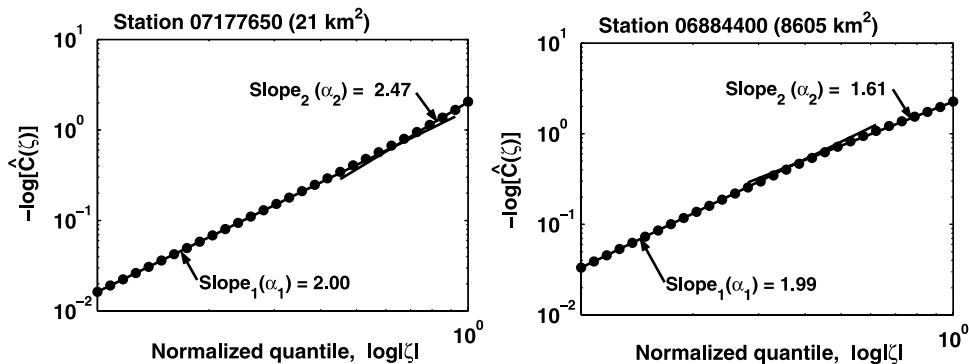


**Figure 8.** Example for log-log fits of two stable distributions.

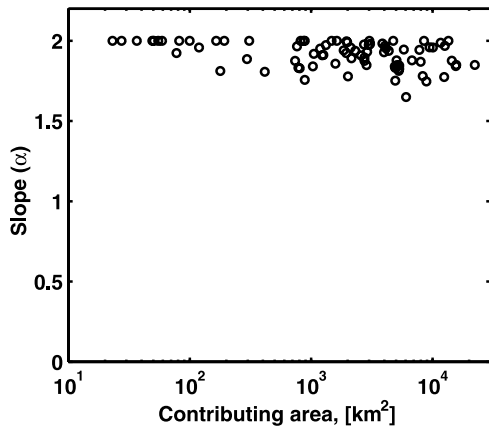


**Figure 9.** Plot of the characteristic exponent  $\alpha$  of the log-Lévy distribution fitted to the daily discharge series of all 85 stations.

from simple scaling in  $C_A$  and  $Q$ ). In contrast, we have observed dependency of these exponents on the contributing area (as presented in Figure 6).

[29] A primary indicator for multiscaling is the behavior of the coefficient of variation (a normalized surrogate for variability) at a station,  $CV(A_j)$  as a function of contributing area [Smith, 1992; Gupta et al., 1994]. A constant  $CV$  implies simple scaling (no change of variability with scale), while an increasing (decreasing)  $CV$  with scale implies multiscaling with increasing (decreasing) variability with scale (see also Appendix A). In Figure 13 we plot  $CV(A_j)$  versus contributing area for  $C_A$ ,  $Q$ , and  $V$  as estimated directly from observations (points) and as predicted by the fitted multiscaling models for  $Q$ ,  $C_A$  and the derived model for  $V$  (lines). The coefficient of variation of discharge exhibits a lot of spread with negligible increase within the whole range of data (implying that a simple scaling model would have been a good approximation). The trend in  $CV$  of cross-sectional area is toward an increase with contributing area, while the coefficient of variation of velocity shows decreasing trend with scale. It is emphasized that the  $CV$  lines in Figure 13 are

**Table 3.** Parameters of the Fitted Lognormal Multiscaling Models

Hydraulic Geometry Factors	Estimated Model Parameters			
	$\alpha$	$\beta$	$\gamma$	$\delta$
<i>Simple Scaling</i>				
Cross-sectional area $C_A$	-3.1802	0.6124	1.1404	0.0000
Discharge $Q$	-5.5428	0.7992	2.2134	0.0000
<i>Multiscaling</i>				
Cross-sectional area $C_A$	-3.1802	0.6124	0.8404	0.1130
Discharge $Q$	-5.5428	0.7992	2.6134	0.0012

not LS fitted to the  $CV$ s computed directly from observations but rather derived from the multiscaling models which have been LS fitted to 10 quantiles of  $C_A$  and  $Q$  simultaneously as explained above. The agreement of the corresponding multiscaling model computed  $CV$ s with the empirical at-station  $CV$ s is satisfactory for the discharge and cross-sectional area, while the derived  $CV$ s of the velocity are slightly overestimates, especially for large scales. It is noted that if simple scaling models were hypothesized for  $C_A$  and  $Q$ , a simple scaling model would have resulted for  $V$  (see section 3.4), implying a constant theoretical  $CV$  for  $V$ . As seen from Figure 13, the empirical observations for  $V$  would not have supported such a hypothesis.

[30] Finally, in Figure 14 we plot the first two moments of the observations of  $C_A$ ,  $Q$  and  $V$  computed at each station  $j$  versus the contributing area  $A_j$  and compare them to the ones predicted by the corresponding lognormal multiscaling models  $\ln E[\Lambda^n(A)] = n\alpha_\Lambda + 0.5n^2\gamma_\Lambda + (n\beta_\Lambda + 0.5n^2\delta_\Lambda)\ln A$  (see Appendix A and Gupta et al. [1994]), where  $\Lambda$  denotes  $Q$  or  $C_A$  and the moments of  $V$  derived through the multiscaling models of  $Q$  and  $C_A$ . Again, the agreement is quite good with more scatter in the plots of variances.

**3.3. Generalized HG Based on Multiscaling**

[31] Considering the equivalency of velocity, cross-sectional area and discharge quantiles postulated by equation (4) we can solve equation (2) for  $z_p$  and combine equation (2a) with equation (2b) in order to derive scale-

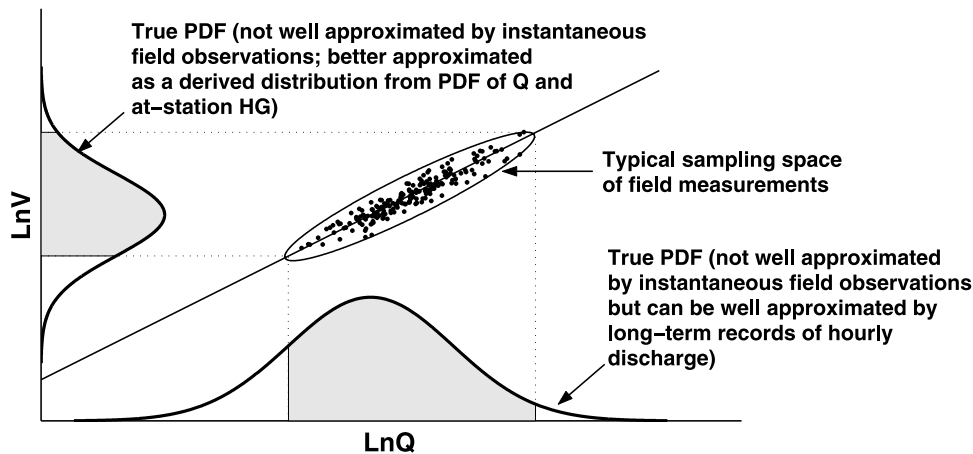


**Figure 10.** At-station  $\ln V$  versus  $\ln Q$  relationship and illustration of the fact that available instantaneous observations of  $V$  and  $Q$  do not usually sample the full probability spaces of these variables and therefore cannot provide good approximations of their true PDFs. Since the true PDF of instantaneous  $Q$  can be well approximated by analysis of long-term records of hourly or daily discharge, a good approximation of the true PDF of  $V$  can be obtained via a derived approach.

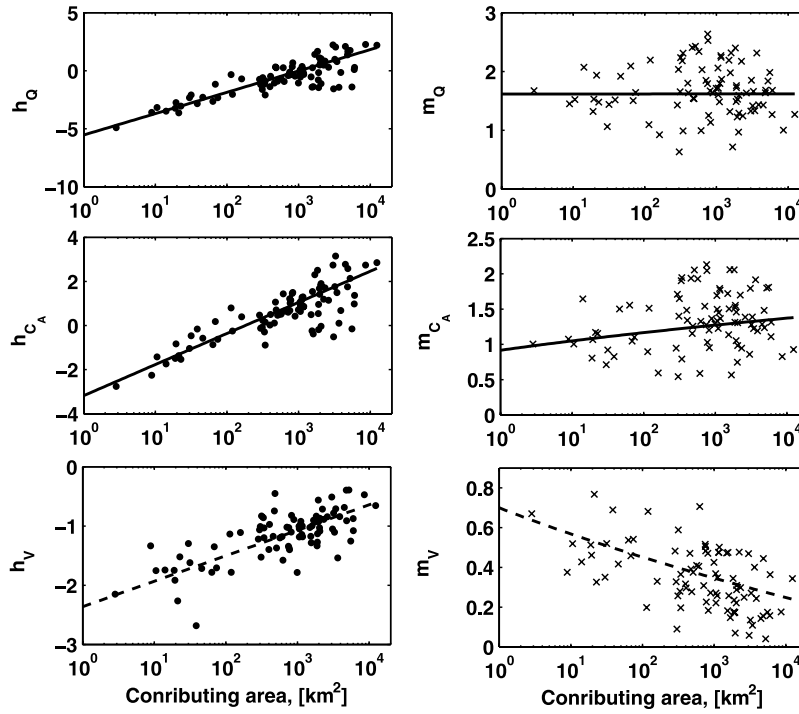


**Figure 11.** Plots of at-station estimates of  $h_{\Lambda}(A_j)$  and  $m_{\Lambda}(A_j)$  (where  $\Lambda$  denotes  $C_A$ ,  $Q$  or  $V$ ) versus contributing area  $A_j$  for each of the  $j$ th station. The points correspond to the empirical estimates of these quantities (which are nothing but the means and standard deviations of the logs of  $C_A$ ,  $V$  and  $Q$ , respectively). The solid lines are the theoretical quantities predicted by the multiscaling models i.e.,  $h_{\Lambda}(A_j) = \alpha_{\Lambda} + \beta_{\Lambda} \ln A_j$  and  $m_{\Lambda}(A_j) = (\gamma_{\Lambda} + \delta_{\Lambda} \ln A_j)^{1/2}$ , while the dashed lines represent the derived estimates for the velocity. It is seen that the fitted multiscaling models explain well the observed empirical trends.

dependent at-station relationships between  $C_A$ ,  $V$  and  $Q$  similar to the *Leopold and Maddock* [1953] power laws:

$$C_{A_p} = \Phi_{C_A}(A) Q_p^{\Psi_{C_A}(A)} \quad (8a)$$

$$V_p = \Phi_V(A) Q_p^{\Psi_V(A)} \quad (8b)$$

where

$$\Psi_{C_A}(A) = \left( \frac{\gamma_{C_A} + \delta_{C_A} \ln A}{\gamma_Q + \delta_Q \ln A} \right)^{1/2} \quad (9a)$$

$$\Phi_{C_A}(A) = \exp[(\alpha_{C_A} + \beta_{C_A} \ln A) - (\alpha_Q + \beta_Q \ln A) \Psi_{C_A}] \quad (9b)$$

$$\Psi_V(A) = 1 - \Psi_{C_A}(A) \quad (9c)$$

$$\Phi_V(A) = 1/\Phi_{C_A}(A) \quad (9d)$$

[32] In Figure 15 the values of HG slopes and intercepts empirically estimated from the at-station log-log linear plots of  $V$  and  $C_A$  versus discharge  $Q$  are plotted as a function of contributing area for the 85 available stations. On the same plots, the theoretical curves  $\Phi_{C_A}(A)$ ,  $\Psi_{C_A}(A)$ ,  $\Phi_V(A)$ ,  $\Psi_V(A)$ , computed from equation (9) using the fitted parameters from Table 3 have been plotted. We see that the empirical values agree well with the theoretical values predicted by equation (9), thus further validating the proposed multiscaling model for hydraulic geometry. The results of *Stall and Fok* [1968] are also plotted for comparison. The agreement between the two analyses is not surprising considering the fact that the topographic and climatic characteristics of the two regions are similar.

[33] Analytical derivation of the parameters of the downstream HG is not possible, but these can easily be evaluated numerically. In Figure 16 we plot the downstream hydraulic geometry for two different frequencies of exceedance 1 and 90%. The agreement between the empirical downstream HG and the theoretically predicted HG from the corresponding multiscaling models is quite good.

[34] Our conclusion from the above analysis is that the proposed multiscaling formalism for HG explains well both the at-station and downstream hydraulic geometry for cross-sectional area, discharge and velocity. Having explicit relationships of HG in terms of scale and frequency gives the possibility of coupling channel hydraulics and the topologic structure of the stream network into a routing model such as the one described later in Section 4 and Appendix C. In the next section, the multiscaling formalism for HG is contrasted with the classical HG of *Leopold and Maddock* [1953] and is shown that the classical HG results as a special case of the proposed formalism.

### 3.4. Classical HG as a Special Case of the Multiscaling Formalism

[35] It is noted that if the parameter  $\delta$  in equation (2) is zero, then the multiscaling models for  $C_A$  and  $Q$  collapse to simple scaling and take the form:

$$\ln C_{A_p}(A) = (\alpha_{C_A} + \beta_{C_A} \ln A) + \sqrt{\gamma_{C_A}} z_p, \quad (10a)$$

$$\ln Q_p(A) = (\alpha_Q + \beta_Q \ln A) + \sqrt{\gamma_Q} z_p \quad (10b)$$

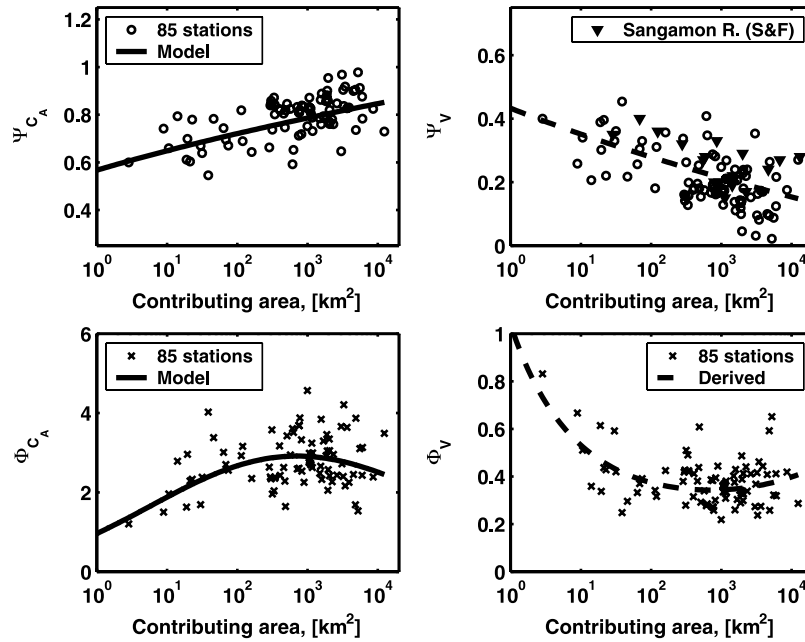


**Figure 12.** Plot of the logarithms of  $C_{A_p}^j$ ,  $Q_p^j$  and  $V_p^j$  computed independently at each station  $j$  of area  $A_j$  for two different frequencies (points) compared to the theoretically derived lines corresponding to the lognormal multiscaling models (equations (2a), (2b), and (5a)).

[36] Using the above equations, the HG for  $C_A$  and  $V$  can be derived as

$$C_{A_p} = \Phi_{C_A}(A)Q_p^{\Psi_{C_A}} \quad (11a)$$

$$V_p = \Phi_V(A)Q_p^{\Psi_V} \quad (11b)$$

where

$$\Psi_{C_A} = \sqrt{\gamma_{C_A}/\gamma_Q} \quad (12a)$$

$$\Phi_{C_A}(A) = \exp[(\alpha_{C_A} + \beta_{C_A} \ln A) - (\alpha_Q + \beta_Q \ln A)\Psi_{C_A}]$$

and

$$\Psi_V = 1 - \Psi_{C_A} \quad \Phi_V(A) = 1/\Phi_{C_A}(A) \quad (12b)$$

[37] It is noted that the exponent of the log-log linear relationship of cross-sectional area and velocity with discharge does not depend on scale but only the intercept. It is therefore seen that simple scaling in  $C_A$  and  $Q$  results in the classical HG.

[38] Despite the fact that the parameters  $\alpha$  and  $\beta$  are the same for both multiscaling and simple scaling models, a new separate fit is necessary for estimation of the parameter  $\gamma$  in the simple scaling model (once  $\delta$  has been set to zero). It is interesting to note that the velocity HG exponent of equation (12b) comes out to be 0.28 when the values of the average exponents and preexponents (i.e.,  $\Phi = 0.21$  and  $\Psi = 0.38$ ) from Table 1 are used. This exponent is not far from the value of  $m = 0.34$  of *Leopold and Maddock* [1953] and is comparable to the average value of the velocity HG exponent for the region of study (see Table 1 for the average value of  $m$ ).

[39] It is also noted that since for a normal distribution the probability of exceedance  $F$  in the interval between 0.1 and 0.9 can be approximated linearly by the standard normal quantile  $z_p$ , the Stall and Fok equations (1b) and (1c) can be written as

$$\ln C_A(F, A) = \alpha''_{C_A} + \beta''_{C_A} z_p + \gamma''_{C_A} \ln A \quad (13a)$$

$$\ln Q(F, A) = \alpha''_Q + \beta''_Q z_p + \gamma''_Q \ln A \quad (13b)$$

which are simple scaling models (variability does not change with scale) and a special case of the multiscaling models of equations (2a) and (2b). It is also noted that if in the above equations the coefficients  $\gamma''$  are linear functions of  $z_p$ , a special form of multiscaling dependence arises, e.g.,

$$\begin{aligned} \ln C_{A_p}(A) &= (\alpha'''_{C_A} + \beta'''_{C_A} z_p) + (\gamma'''_{C_A} + \delta'''_{C_A} z_p) \ln A \\ &= (\tilde{\alpha}'''_{C_A} + \tilde{\beta}'''_{C_A} \ln A) + (\tilde{\gamma}'''_{C_A} + \tilde{\delta}'''_{C_A} \ln A) z_p \end{aligned} \quad (14)$$

This multiscaling dependence is a special case of equation (2) for  $\alpha = 1$  (Cauchy distributions). Notice that in contrast to equation (2), in the case of equations (13) and (14), i.e., simple scaling for  $C_A$  and  $Q$ , a multiscaling model for  $V$  also exists, such that its parameters can be expressed in terms of the multiscaling parameters of  $C_A$  and  $Q$ .

#### 4. Classical Versus Generalized HG: Effect on Hydrologic Response

[40] Since the time necessary for a particle to travel a reach of unit length is inversely related to the mean velocity, a possible consequence of scale-dependent HG exponents is that the parameters of the hydrographs (e.g., peak flow, lag

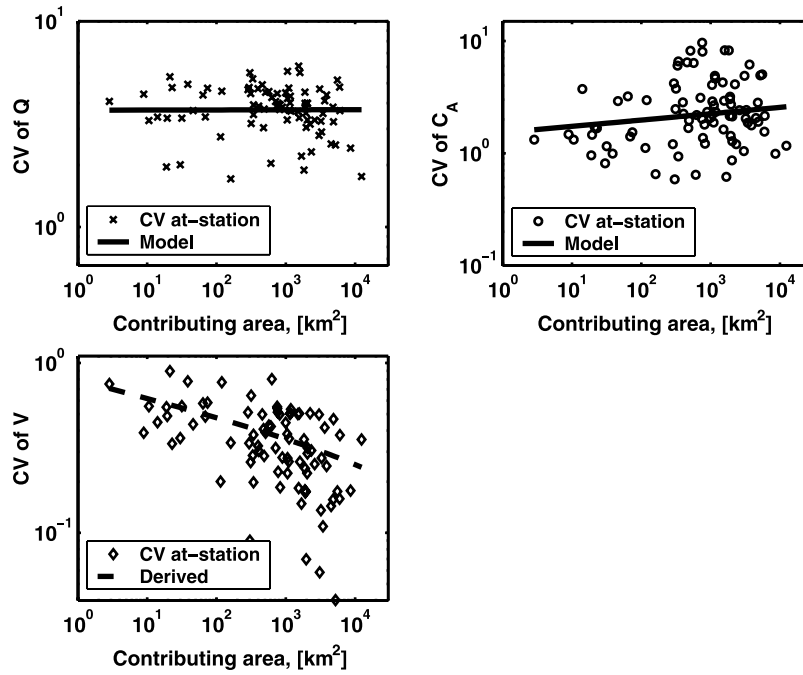


**Figure 13.** Plot of at-station coefficients of variation ( $CV$ ) of discharge ( $Q$ ), cross-sectional area ( $C_A$ ), and mean velocity ( $V$ ) versus contributing area. Points indicate values estimated directly from observations, solid lines show the theoretical curves predicted by the multiscaling models, and dashed line represents the derived curve for velocity.

time, mean holding time etc.) of catchments with different contributing areas will increase or decrease with different rates for the same increase in the input. Empirical evidence supports this hypothesis (e.g., see *Minshall* [1960] for peak flows, *Boyd et al.* [1979] for lag times, and *Wang et al.* [1981] for mean holding times), where the relationship

between the magnitude of the rainfall input  $I_0$  and the hydrograph parameter  $P$  followed a power law in the form  $P \sim I_0^{-\alpha}$ , with an exponent depending on contributing area (scale). Such a trend is not reproduced by previous studies coupling geomorphologic analyses and HG with constant exponents [e.g., *Saco and Kumar*, 2002b, equation (22)].

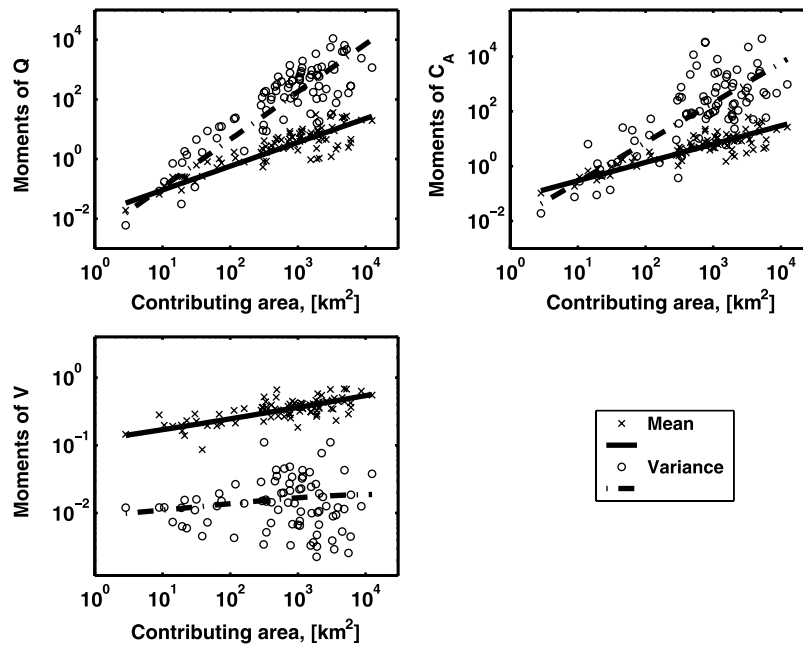


**Figure 14.** Comparison of first two moments of  $Q$ ,  $C_A$ , and  $V$  at a station to the theoretical moments given by the relationship  $\ln E[\Lambda^n(A)] = n\alpha_\Lambda + 0.5n^2\gamma_\Lambda + (n\beta_\Lambda + 0.5n^2\delta_\Lambda)\ln A$ , where  $\Lambda$  denotes  $C_A$  or  $Q$ . The theoretical moments of  $V$  are derived through the relationship  $\ln V = \ln Q - \ln C_A$ .

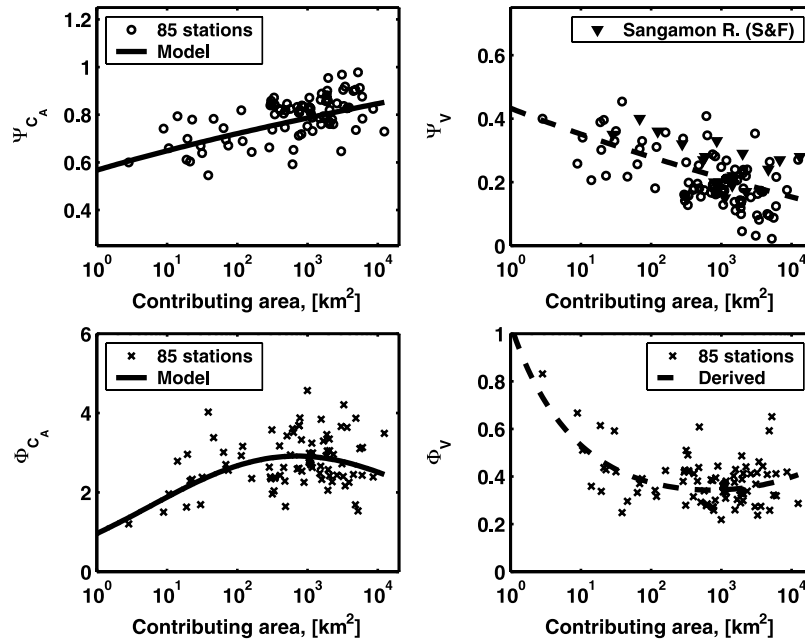


**Figure 15.** At-station (top) fitted exponents and (bottom) preexponents for cross-sectional area and velocity (i.e., parameters of the fitted *Leopold and Maddock's* [1953] power laws) for the 85 stations versus their contributing area (notice that the top plots are the same as Figure 6), but now the theoretical curves  $\Phi_{C_A}(A)$ ,  $\Phi_V(A)$ ,  $\Psi_{C_A}(A)$  and  $\Psi_V(A)$  derived from the proposed multiscaling model (equations (9)) have also been plotted. The good agreement further verifies that the proposed generalized model for HG nicely explains the empirical trends.

We will demonstrate that the generalized HG we propose reproduces this trend.

[41] Specifically, in this section we quantify hydrologic response by assuming the classical HG (which as was shown in the previous section results from simple scaling in HG factors) versus the proposed generalized HG (which results from multiscaling). The numerical experiment performed to quantify the above is as follows. A forcing (effective rainfall) is assumed to uniformly cover the whole basin and have an intensity  $I$  over a short time interval  $\Delta t$  (instantaneous pulse). The properties of the channel network (see Appendix B) have been assumed to be (1) Horton's ratios  $R_L = 2$  and  $R_A = 5$  representing the average values observed in natural river basins [see *Rodríguez-Iturbe and*

*Rinaldo*, 1997, chap. 7], (2) mean contributing area and mean channel length of streams of order 1,  $\bar{A}_1$  and  $\bar{L}_1$  are assumed respectively  $\bar{A}_1 = 0.02 \text{ km}^2$  and  $\bar{L}_1 = 0.2 \text{ km}$  and are computed from the geomorphologic analysis of several catchments in Kansas, and (3) tributary structure represented by *Tokunaga* [1966] type of tree generator with parameters  $a = 1$  and  $c = 2$  (which results in bifurcation ratio  $R_B = 4$ ).

[42] For routing, a network of geomorphologic nonlinear reservoirs (similar in nature to the ones of *Boyd et al.* [1979], *Berod et al.* [1995], *Reggiani et al.* [2001], and *Menabde and Sivapalan* [2001]) is used and the routing parameters have been derived in terms of the multiscaling HG model parameters and the properties of the river

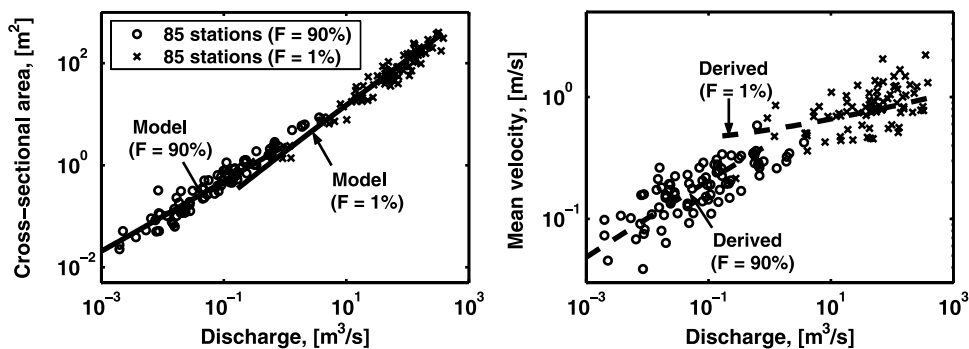


**Figure 16.** Downstream HG for two different frequencies of exceedance  $F$  of streamflow  $Q$ . The points represent empirical values, the solid lines are the theoretically derived curves from the corresponding lognormal multiscaling models for discharge and cross-sectional area (left panel), and the dashed lines represent the derived curves for velocity (right panel).

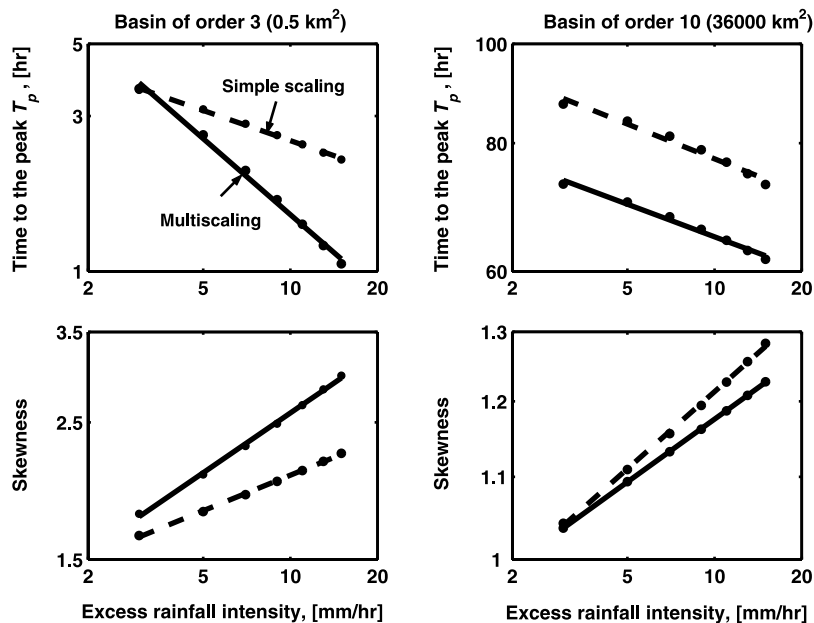


**Figure 17.** Example of power laws between some of the hydrograph parameters and the excess rainfall intensity.

network (see Appendix C). The developed routing scheme is termed Geomorphologic Nonlinear Reservoirs in Network and denoted as GNRN. Although simple, this lumped scheme is suitable for our comparative analysis since its storage-discharge relationships, being explicit functions of the HG, allow a relative comparison of hydrologic response under the assumption of simple scaling HG (which results in constant exponents of storage-discharge relationships with scale) versus multiscaling HG (which results in scale-dependent storage-discharge exponents).

[43] Pulses of varying intensity have been routed through the basin and the hydrographs resulting at the end of basins of different orders (and therefore different contributing areas) have been computed. These hydrographs have been parameterized in terms of some key parameters, such as peak discharge  $Q_{pk}$ , time to the peak  $T_{pk}$ , and the first three central moments of the synthetic hydrographs in order to characterize the shape of the response functions. (Notice that, due to the nonlinear nature of GNRN, we are not allowed to consider the response of a catchment to a unit pulse as a travel time distribution; consequently, the central moments of the response function can only be interpreted as descriptors of the hydrograph's geometry but not as moments of the travel time). The numerical experiment has been repeated for several rainfall intensities  $I$  and the dependence of the hydrograph parameters on the rainfall intensity and contributing area  $A$  has been quantified.

[44] It was found that in both cases of classical and generalized HG, the hydrograph parameters versus effective rainfall intensity can be well approximated by power laws for all order basins. An example of such power laws is demonstrated in Figure 17 for time to peak  $T_{pk}$  and skewness  $S_k$  (as the ratio of the second and third central moments  $S_k$  also follows a power law with  $I$ ) for two hypothetical catchments of orders 3 and 10 and also for classical versus generalized HG. The power law approximations are in general nonlinear in the log-log domain, but

with small curvature still allowing a good log-log linear approximation.

[45] It is noted that even in the simple case of a linear response the emergence of the above power laws cannot be derived analytically. This is due to the fact that basin response is expressed in terms of the sum of exponential functions and the higher-order moments are expressed as the sum of power law functions (for details, see *Rodriguez-Iturbe and Valdes* [1979], *Rodriguez-Iturbe and Rinaldo* [1997], and *Saco and Kumar* [2002a, 2002b]). In the case of GNRN, due to the nonlinear nature of this routing scheme, derivation of the emerging power laws from the theoretical point of view is even more intractable. Nevertheless, the parameters of these approximate power laws are useful “measures” of the dependence of hydrologic response on scale and rainfall input (as suggested by *Wang et al.* [1981]), and we will utilize them in our analysis. We assume the following parameterizations:

$$\text{Peak rate} \quad Q_{pk} = I^{\eta_1(A)} \quad (15a)$$

$$\text{Time to the peak} \quad T_{pk} = I^{\eta_2(A)} \quad (15b)$$

$$\text{Fist central moment} \quad T_m = I^{\eta_3(A)} \quad (15c)$$

$$\text{Skewness} \quad S_k = I^{\eta_4(A)} \quad (15d)$$

[46] Figure 18 shows the exponents  $\eta_1(A)$ ,  $\eta_2(A)$ ,  $\eta_3(A)$  and  $\eta_4(A)$  as functions of contributing area  $A$  for both simple and multiscaling HG models. Clearly, the range in which the exponents vary with contributing area is much wider for the routing based on multiscaling HG, thus suggesting significant nonlinear effects in smaller basins.

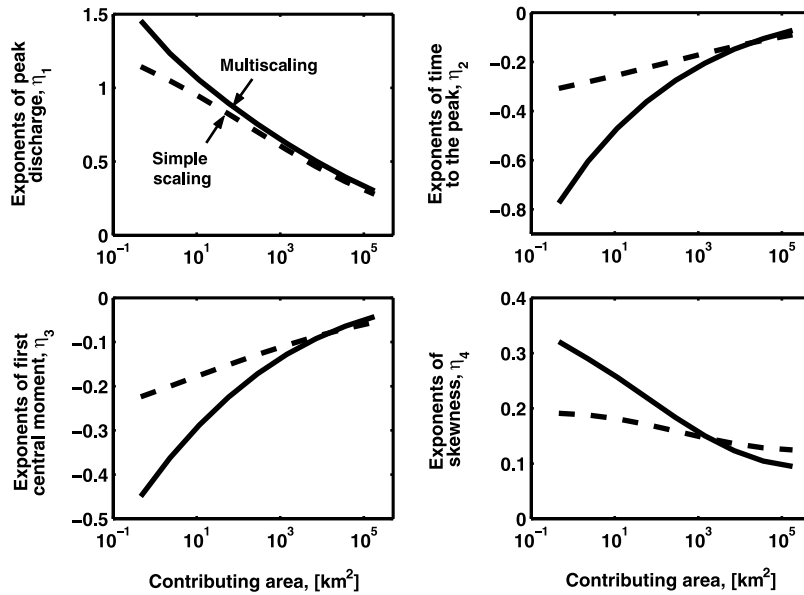


**Figure 18.** Exponents of hydrologic response functions (equations (15)) versus scale.

In other words, the hydrologic response is seen to be significantly influenced by the assumption about HG especially in small basins in which the exponents  $\eta_{(c)}(A)$  show significant differences between classical and generalized HG. It is interesting also to note that the product  $Q_{pk}T_{pk}$ , which under the assumption of constant velocity has been shown to be a scale-invariant quantity [e.g., see *Rodriguez-Iturbe and Valdes, 1979*] is shown here to depend on scale as  $Q_{pk}T_{pk} = I^{\eta_1(A)+\eta_2(A)}$  for both classical and generalized HG. The exponent  $[\eta_1(A) + \eta_2(A)]$  varies from approximately 0.8 for small basins to approximately 0.2 for large basins. Interestingly, the variation of this exponent with scale is not dependent on the nature of HG (that is, it achieves the same values for either simple or generalized HG), although each term of the sum, i.e.,  $\eta_1(A)$  and  $\eta_2(A)$  changes differently with scale in each case.

[47] It is noted that the above results were obtained under the assumption of spatially uniform effective rainfall. Future work should address the issues of spatially variable rainfall. It is possible that the spatial inhomogeneity of effective rainfall, once coupled with the spatial inhomogeneity of channel HG, will dampen the dependence of the degree of nonlinearity on scale on the average (ensemble average), but not in terms of variance. Such numerical experiments need to be performed under realistic scenarios of rainfall variability along the lines of *Menabde and Sivapalan [2001]*.

## 5. Future Extension

[48] Although the lognormal multiscaling model of HG proposed in this paper is a good working model to develop understanding of spatial inhomogeneities and scale frequency dependence of hydrologic response, there are a few observations that suggest some possible extensions worth considering in the future. These observations are (1) there is significant uncertainty in HG relationships in terms of considerable scatter in the log-log plots, (2) a single power law cannot reproduce the change in slope and sometimes discontinuities in HG near bank-full conditions [e.g., see *Pilgrim, 1976; Wong and Laurenson, 1984; Bates,*

*1990*], and (3) a mixed distribution might be needed to represent discharges, especially for both below and above bank-full conditions [e.g., see *Singh and Sinclair, 1972; Leytham, 1984; LeBoutillier and Waylen, 1993*]. Here we propose an extension of the lognormal multiscaling model to a mixed bivariate lognormal multiscaling model which can accommodate the above considerations.

[49] The treatment of uncertainty in hydraulic geometry comes very naturally in the proposed multiscaling framework by extending it to account for the covariance between  $\ln Q$  and  $\ln C_A$  (or  $\ln V$ ). In this context, a single at-station power law relationship can be represented by introducing a bivariate Gaussian distribution of  $\ln C_A$  and  $\ln Q$  (or  $\ln V$  and  $\ln Q$ ) and considering the conditional expectation  $E[\ln C_A | \ln Q]$  for a wide range of possible discharges. Furthermore, assuming that the covariances of  $\ln Q$  and  $\ln C_A$  (or  $\ln V$ ) are linearly dependent on the log of contributing area (as it is for their variances), we can extend our multiscaling framework to a mixed bivariate multiscaling lognormal model in the form:

$$Y = pY_1 + (1-p)Y_2 \quad (16)$$

[50] In equation (16)  $p$  is the mixing proportion (for example the percentage of time in which the discharge is less than bank-full), and  $Y_1$  and  $Y_2$  are bivariate multiscaling models in the form:

$$Y \sim N(\mathbf{M}_\alpha + \mathbf{M}_\beta \ln A, \Sigma_\alpha + \Sigma_\beta \ln A) \quad (17)$$

where

$$\mathbf{Y} = [\ln Q \ln \Lambda]^T, \mathbf{M}_\alpha = [\alpha_{1,Q} \alpha_{1,\Lambda}]^T, \mathbf{M}_\beta = [\beta_{1,Q} \beta_{1,\Lambda}]^T, \\ \Sigma_\alpha = \begin{bmatrix} \alpha_{2,Q} & \alpha_{2,Q\Lambda} \\ \alpha_{2,Q\Lambda} & \alpha_{2,\Lambda} \end{bmatrix}, \Sigma_\beta = \begin{bmatrix} \beta_{2,Q} & \beta_{2,Q\Lambda} \\ \beta_{2,Q\Lambda} & \beta_{2,\Lambda} \end{bmatrix}$$

and  $\alpha_{m,(c)}$  is the intercept and  $\beta_{m,(c)}$  the slope of the linear fit of  $m$ th-order moments of  $Q$  and  $C_A$  (or  $V$ ) versus  $\ln A$  ( $C_A$  and  $V$  are denoted as  $\Lambda$  and the coefficients corresponding to the covariance are  $\alpha_{2,Q\Lambda}$  and  $\beta_{2,Q\Lambda}$ ).

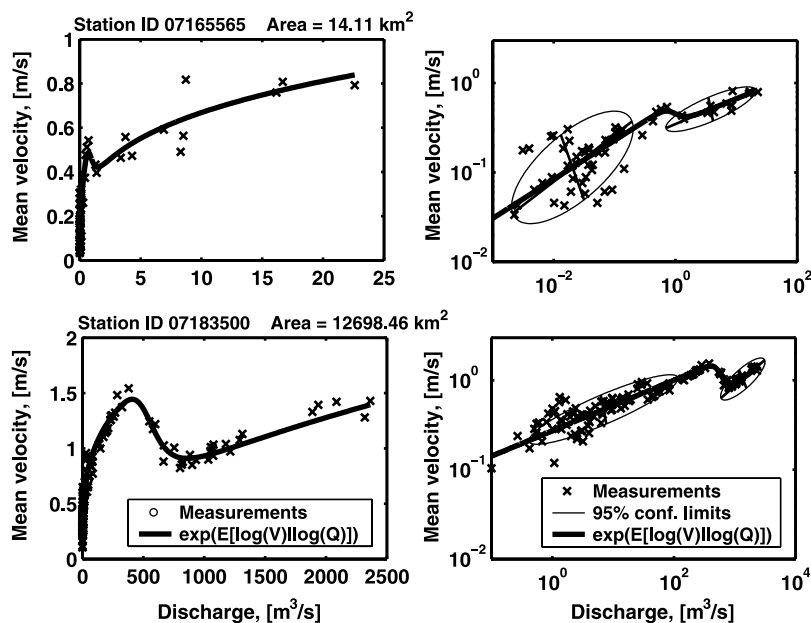


**Figure 19.** Representation of at-station HG as a mixture of two bivariate Gaussians with contributions 99 and 1%, respectively. Two different size basins are considered: small ( $\approx 14 \text{ km}^2$ ) and large ( $\approx 12,700 \text{ km}^2$ ).

[51] Figure 19 shows several examples of bivariate Gaussian mixture models fitted (through an expectation maximization algorithm [e.g., see *McLachlan and Krishnan, 1997*]) to at-station data for mean velocity and discharge for two basins of areas  $14 \text{ km}^2$  and  $12,700 \text{ km}^2$ . It is noted that the previously considered lognormal multiscaling framework simply assumed that the log-log plots of velocity versus discharge (right-hand panels in Figure 19) could be approximated by a single power law relationship. Although the single power law might not be a bad overall approximation, the systematic deviations at high discharges are notable.

[52] The proposed extended model (equations (16) and (17)) has been fitted to our data from all 85 stations and the exponent of the obtained conditional expectation  $\exp\{E[\ln V | \ln Q]\}$  for a wide range of discharges has been used to represent the at-station HG. Figure 20 shows the computed at-station HG for 2 basins of size 10 and  $10,000 \text{ km}^2$  and also the downstream HG for two different frequencies of discharge. The model shows behavior similar to that observed in many empirical studies [e.g., see *Carlston, 1969; Pilgrim, 1976; Wong and Laurenson, 1984*], i.e., close to log-log linear relationship for downstream HG (right panels in Figure 20), and two log-log linear relationships for at-station HG with a proper treatment of the transition in between below and above bank-full conditions.

[53] The proposed framework is expected to provide a more reliable representation of at-station and downstream HG and is attractive for analysis of the hydrologic response of basins for both below and above bank-full conditions. Furthermore, it provides a stochastic representation of HG, which explicitly acknowledges the uncertainty in these relationships. Another important feature of the proposed extension is that the full complexity of the flood propagation in a stream network is represented with a relatively parsimo-

nious model. This could allow regionalization and even parameter transfer between regions with similar climatic, topographic and geologic conditions.

## 6. Summary and Conclusions

[54] Empirical evidence has been presented that the exponents of at-station HG systematically depend on scale and the exponents of downstream HG on frequency. To explain this empirical finding, a multiscaling formalism within which to model and interpret HG has been proposed. Specifically, a lognormal multiscaling model has been suggested for representing hydraulic geometry factors of a stream channel (discharge  $Q$  and cross-sectional area  $C_A$ ). This multiscaling model has then been used to analytically derive revised at-station hydraulic geometry (HG, i.e., relationships between  $C_A$  and  $Q$  and  $V$  and  $Q$ ) whose coefficients are explicit functions of scale (contributing area). It has also been used to numerically derive revised downstream HG, as an analytical derivation in terms of the multiscaling model parameters is impossible in this case. The generalized HG model has been fitted to 85 gauging stations in Oklahoma and Kansas, and has been shown to explain, to a good degree, the empirical trends.

[55] An important consequence of scale-dependent at-station HG is the implied spatial heterogeneity in catchment hydrologic response. This is because different parts of the basin will respond to the same rainfall forcing in ways that depend on their location (and thus the area drained above). Via a network of geomorphologic nonlinear reservoirs routing model, we demonstrated the effect of spatially uniform channel response (implied by the classical HG whose exponents remain constant with scale) and the scale-dependent channel response (resulting from the proposed generalized HG whose exponents are functions of scale). Important differences on the hydrologic response function (time to

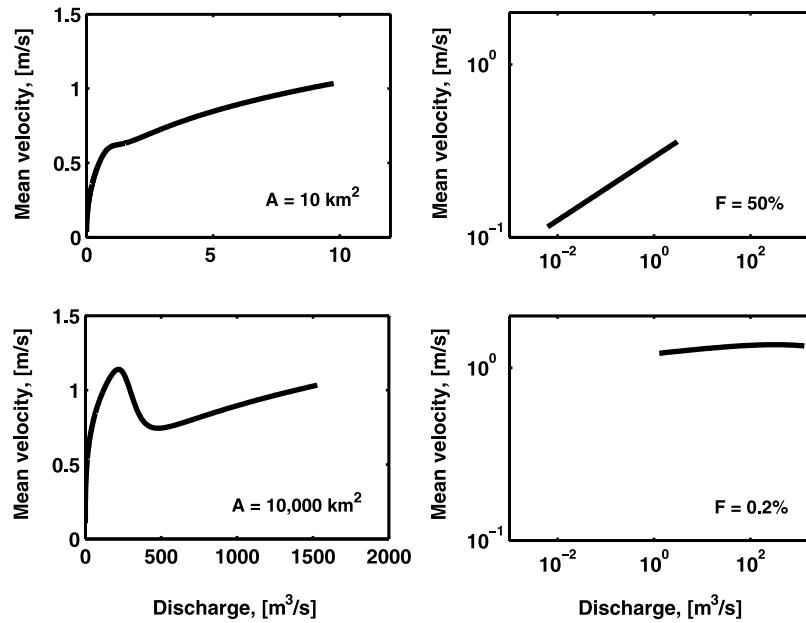


**Figure 20.** An illustrative example showing how a mixed bivariate lognormal multiscaling model can be used to represent a general relationship  $V = f(Q)$ : (left) at-station HG for different contributing areas and (right) downstream HG for different frequencies of discharge.

peak, peak discharge and skewness of the hydrograph) are noted prompting the need to further study the physical origin of these scale dependencies especially for small basins.

[56] In their seminal work, *Leopold and Maddock* [1953] provided important quantifications of how stream hydraulics and morphometric properties relate to discharge in an average sense, i.e., by ignoring much of the scattering around the proposed power laws, and capturing only general trends. They commented that “further work will be necessary to explain the details of deviations from these trends” [*Leopold and Maddock*, 1953, p. 10]. We see our work as providing an explanation of some of these deviations by attributing them to systematic dependencies on scale and frequency. As such, the proposed generalized HG (which includes the classical HG as a special case) makes a small step toward the problem of quantifying the scale-dependent (and thus spatially heterogeneous) response of catchments. An important subsequent problem is to understand the physical origin of this scale dependence. Some thoughts on this problem are offered by B. A. Dodov and E. Foufoula-Georgiou (Generalized hydraulic geometry: Insights based on instability analysis and a physical model, submitted to *Water Resources Research*, 2004) based on fluvial instability analysis and a physical model of meandering rivers.

## Appendix A: Review of the Multiscaling Formalism

[57] We present a brief review of the multiscaling theory following *Gupta and Waymire* [1990] and *Gupta et al.* [1994]. A random field  $\{X(A)\}$  parameterized by a scale parameter  $A$ , e.g., drainage area, is said to exhibit multiscaling if it satisfies the following equality under a change of scale

$$X(\lambda A) = G(\lambda)X(A) \quad (\text{A1})$$

where  $\lambda > 0$  is a dimensionless scalar, e.g., the ratio of drainage areas,  $G(\lambda)$  is a positive random or nonrandom function and  $=$  denotes equality in probability distributions. Equation (A1) implies that the probability distribution of  $X(\lambda A)$  can be determined from that of  $X(A)$  provided that the function  $G(\lambda)$  is known.

[58] Simple scaling is said to hold when  $G(\lambda)$  is a non-random function. In this case, it can be shown that  $G(\lambda) = \lambda^\Theta$ , and that the quantiles  $X_p(A)$ , defined as  $P\{X(A) > X_p(A)\} = p$ , of  $\{X(A)\}$  relate to  $A$  in a power law form, i.e.,

$$X_p(A) = c(p)A^\Theta, \quad (\text{A2})$$

where  $c$  and  $\Theta$  are parameters independent of scale [see *Gupta and Waymire*, 1990]. Simple scaling results in a coefficient of variation ( $CV$ ) which is independent of scale. Regarding  $CV$  as a measure of spatial variability, simple scaling implies spatial homogeneity in terms of a constant variability with scale.

[59] Multiscaling is said to hold when  $G(\lambda)$  is a random function. Unlike simple scaling, multiscaling admits two representations of  $G(\lambda)$  corresponding to whether  $\lambda > 1$  or  $\lambda < 1$ . As has been shown by *Gupta and Waymire* [1990], these two cases correspond, respectively, to an increasing or decreasing  $CV$  with scale. In either case, it can be shown that the random function  $G(\lambda)$  can be expressed in terms of scale  $\lambda$  and a Lévy stable random variable,  $w_p$ . Also, the quantiles of the process can be written as

$$\ln X_p(A) = (a \pm \beta \ln A) + (\gamma \pm \delta \ln A)^{1/\alpha} w_p, \quad \lambda > 1 \text{ or } \lambda < 1 \quad (\text{A3})$$

where  $\alpha$ ,  $\beta$ ,  $\gamma$  and  $\delta$  are appropriately specified parameters [see *Gupta and Waymire*, 1990] and  $w_p$  denotes the  $p$ th quantile of  $-W$ , where  $W$  is a Lévy-stable random variable

with characteristic exponent  $0 < \alpha \leq 2$ . The special case of  $\alpha = 2$  corresponds to the so-called lognormal multiscaling model.

[60] *Gupta and Waymire* [1990] show that in the case of decreasing  $CV$  with increasing scale ( $\lambda < 1$ ), a limiting approximation of equation (A3) can be obtained for large scales, which brings the quantiles in a log-log linear form

$$X_p(A) = c(p)A^{\Theta(p)} \quad (A4)$$

where the exponents and intercepts are functions of the quantile and the other parameters of the model. In the case of increasing  $CV$  with scale ( $\lambda > 1$ ), no such approximation can be obtained for equation (A3), and the quantiles scale with area in a complex, non log-log linear way.

[61] It is important to mention that the multiscaling theory, as presented above, was developed by *Gupta and Waymire* [1990] in the context of scaling in “floods” (defined as the highest peak discharges recorded each year). Here we invoke the multiscaling theory for channel hydraulic factors such as instantaneous cross-sectional area, velocity etc. and for instantaneous or daily discharges which are of much lower frequency than maximum annual floods. Therefore important differences arise in the interpretation of scaling and these are discussed below. In the study of *Gupta and Waymire* [1990] the two solutions of the scaling function  $G(\lambda)$  were studied in the context of interpreting the empirical observation that the  $CV$  of floods increases with scale  $A$  up to some critical scale  $A_c$  (i.e., for  $A: A^0 < A < A_c$ ) and then decreases (i.e., for  $A_c < A < A^1$ ). Therefore the cases of  $\lambda > 1$  ( $\lambda = A/A^0$ ) and  $\lambda < 1$  ( $\lambda = A/A^1$ ) were given the interpretation of “small” and “large” basins, relatively to the critical basin at which scaling breaks.

[62] In the context that we use multiscaling for, no scaling break is observed and increasing or decreasing variability with increasing scale ( $\lambda > 1$  or  $\lambda < 1$ , respectively) is observed within the same range of scales depending on the variable analyzed. For example, the empirical coefficient of variation of cross-sectional areas shows an increase with scale whereas the coefficient of variation for velocities shows a decrease with scale, both within the same range of scales, 10 to  $10^4$  km<sup>2</sup>.

## Appendix B: Ordering and Mean Self-Similarity of Stream Networks

[63] Stream network ordering of a drainage network can be achieved either starting from the outlet and moving upstream or starting from each source and moving downstream. The most widely used scheme of ordering (utilized in this work) belongs to the second group and was proposed by *Horton* [1945] and revised by *Strahler* [1952, 1957]. The analysis of the stream network proceeds as follows [*Rodriguez-Iturbe and Rinaldo*, 1997]: (1) channels that originate at a source (have no tributaries) are defined to be first-order streams; (2) when two streams of order  $\omega$  meet, a stream of order  $\omega + 1$  is created; (3) when two streams of different order meet, the channel segment immediately downstream is assigned the higher order of the two combining streams.

[64] For almost any geometric or topological quantity  $X_\omega$  of streams of order  $\omega$  (e.g., total number, length, contribut-

ing area, number of side tributaries of order less than  $\omega$ , etc.) a power law holds in the form:

$$\langle X_\omega \rangle \propto R_X^\omega \quad (B1)$$

where  $\langle \cdot \rangle$  denotes ensemble average and the constant  $R_X$  is respectively referred to as stream number (or bifurcation) ratio, length ratio, etc. Empirical laws of this generic form are known collectively as “Horton’s laws”, although they are not all due to Horton [e.g., see *Schumm* [1956] for the law of basin areas).

[65] *Peckham* [1995a, 1995b], on the basis of previous work of *Tokunaga* [1966, 1978], introduced a general definition of topologic mean self-similarity for a class of stream network trees where every stream of order  $\omega$  has  $b \geq 2$  upstream tributaries of order  $(\omega - 1)$  and on the average  $T_{\omega,k}$  side tributaries of order  $k$ , ( $\omega \in \{2, \dots, \Omega\}$ ,  $k \in \{1, \dots, \omega - 1\}$  and  $\Omega$  denotes the order of the network). The number of side tributaries  $T_{\omega,k}$  can be arranged in a square, lower triangular matrix

$$T = \begin{pmatrix} T_{2,1} & 0 & 0 & \cdots & 0 \\ T_{3,1} & T_{3,2} & 0 & \cdots & 0 \\ T_{4,1} & T_{4,2} & T_{4,3} & \cdots & 0 \\ \vdots & \vdots & \vdots & \ddots & \vdots \\ T_{\Omega,1} & T_{\Omega,2} & T_{\Omega,3} & \cdots & T_{\Omega,\Omega-1} \end{pmatrix} \quad (B2)$$

[66] Topologically mean self-similar trees are then defined as the subclass of trees with generators that satisfy the constraint that  $T_{\omega,\omega-k} = T_k$ , where  $T_k$  is a number that depends on  $k$  but not  $\omega$ , and gives the number of side tributaries of order  $(\omega - k)$  for every  $\omega > k$ . With several examples, *Peckham* [1995a] showed that this constraint holds fairly well for natural river networks.

[67] For binary trees, two streams of order  $\omega$  must head each stream of order  $(\omega + 1)$ . However, streams of order  $\omega$  also appear as side tributaries to any stream of order greater than  $\omega$ . These facts imply that if  $N_\omega$  is the number of all streams of order  $\omega$ , the following recursive formula must hold [*Peckham*, 1995a, 1995b]:

$$N_\omega = 2N_{\omega+1} + \sum_{k=1}^{\Omega-\omega} T_k N_{\omega+k} \quad (B3)$$

[68] Therefore the sequence  $\{N_\omega\}$  for a binary tree is uniquely determined once the sequence  $\{T_k\}$  has been specified.

## Appendix C: Derivation of Geomorphologic Nonlinear Reservoirs in Network (GNRN) Runoff Routing Model in Terms of HG and Network Topology

### C1. Catchment Representation in Terms of Nonlinear Reservoirs

[69] The purpose of this representation is to define a network of nonlinear reservoirs (which form conceptual building blocks for runoff routing) in terms of Strahler

stream ordering (see Appendix B for background). This formulation will allow us to combine the developed statistical model for hydraulic geometry and the stream network organization, in order to derive the parameters of the nonlinear reservoirs.

[70] Our definition of ‘‘Geomorphologic Nonlinear Reservoirs in Network’’ (GNRN) is based on the following assumptions. (1) All channels of particular order  $\omega$  in a catchment of order  $\Omega$  represent a reservoir of order  $\omega$ , denoted as  $R_\omega$ . (2) At any particular instant in time, the mean velocity is the same in all channels of order  $\omega$  and any input into reservoir of order  $\omega$  is instantaneously redistributed uniformly among all channels of order  $\omega$ . (3) The flow from any reservoir  $R_k$  to any other reservoir  $R_\omega$ ,  $k < \omega$ ,  $k = 1, \dots, \Omega - 1$ ,  $\omega = 2, \dots, \Omega$  is given as

$$Q_{k,\omega} = p_{k,\omega} Q_k^{tot} \quad (C1)$$

where  $Q_k^{tot}$  is the total output from  $R_k$  and  $p_{k,\omega}$  is the proportion of all channels of order  $k$  draining to channels of order  $\omega$ . (4) Differences between contributing areas of all channels of order  $\omega$  are negligible. (5) Equations (2a) and (2b) are assumed to represent distributions of instantaneous quantities.

## C2. Derivation of the Parameters of the Nonlinear Reservoirs in Terms of HG

[71] Under assumption 4 we can rewrite (2a) and (2b) in the form

$$\ln C_{A_p}(\bar{A}_\omega) = \alpha_{C_A} + \beta_{C_A} \ln \bar{A}_\omega + (\gamma_{C_A} + \delta_{C_A} \ln \bar{A}_\omega)^{1/2} z_p \quad (C2a)$$

$$\ln Q_p(\bar{A}_\omega) = \alpha_Q + \beta_Q \ln \bar{A}_\omega + (\gamma_Q + \delta_Q \ln \bar{A}_\omega)^{1/2} z_p \quad (C2b)$$

where  $\bar{A}_\omega$  is the average contributing area of channels of order  $\omega$ .

[72] Under assumptions 1, 2, 4, and 5, equation (2) can be used to represent the logarithms of instantaneous storage and outflow from a reservoir of order  $\omega$  as:

$$\ln S_{\omega,p}(\bar{A}_\omega) = \alpha_{C_A} + \ln \bar{L}_\omega + \ln N_\omega + \beta_{C_A} \ln \bar{A}_\omega + (\gamma_{C_A} + \delta_{C_A} \ln \bar{A}_\omega)^{1/2} z_p \quad (C3a)$$

$$\ln Q_{\omega,p}(\bar{A}_\omega) = \alpha_Q + \ln N_\omega + \beta_Q \ln \bar{A}_\omega + (\gamma_Q + \delta_Q \ln \bar{A}_\omega)^{1/2} z_p \quad (C3b)$$

where  $\bar{L}_\omega$  and  $N_\omega$  are respectively the average length and the total number of streams of order  $\omega$ .

[73] Solving equations (C3) for  $z_p$  (this is allowed by equation (4)) and combining them, gives a power law relationship between the outflow and storage in a reservoir of order  $\omega$

$$Q_\omega = \Phi_\omega S_\omega^{\Psi_\omega} \quad (C4a)$$

where

$$\Psi_\omega = \Psi_{C_A}^{-1}(\bar{A}_\omega) = \left( \frac{\gamma_Q + \delta_Q \ln \bar{A}_\omega}{\gamma_{C_A} + \delta_{C_A} \ln \bar{A}_\omega} \right)^{1/2} \quad (C4b)$$

and

$$\Phi_\omega = N_\omega \exp[\alpha_Q + \beta_Q \ln \bar{A}_\omega - (\alpha_{C_A} + \ln \bar{L}_\omega + \ln N_\omega + \beta_{C_A} \ln \bar{A}_\omega) \Psi_\omega] \quad (C4c)$$

[74] Thus we derived the parameters  $\Phi_\omega$  and  $\Psi_\omega$  of the nonlinear reservoir of order  $\omega$  in terms of the parameters of the proposed multiscaling models for  $Q$  and  $C_A$  and the channel network structure. Since equation (C4a) is assumed to represent instantaneous quantities, it can be used as a momentum conservation equation for all channels of order  $\omega$ . Coupled with a continuity equation it completes a closed set of equations for runoff routing.

## C3. Routing Procedure

[75] The routing procedure is based on the continuity equation  $dS_\omega/dt = I_\omega(t) - Q_\omega(t)$  and the outflow-storage relationship  $Q_\omega = \Phi_\omega S_\omega^{\Psi_\omega}$  serving as the momentum equation.  $I_\omega(t)$  is the total input to a reservoir of order  $\omega$ , which under assumption <3> is given by:

$$I_\omega(t) = E_\omega(t) + \sum_{k=1}^{\omega-1} p_{k,\omega} \Phi_k S_k(t)^{\Psi_k}, \quad \text{for } \omega > 1 \quad (C5a)$$

and by

$$I_\omega(t) = E_\omega(t), \quad \text{for } \omega = 1 \quad (C5b)$$

where  $E_\omega(t)$  denotes any external input: rainfall excess, snowmelt, drainage from deep aquifers, etc. contributing to the storage of the  $\omega$ th reservoir at moment  $t$  and  $p_{k,\omega}$  is the proportion of all channels of order  $k$  draining to channels of order  $\omega$ . The output from the  $\omega$ th reservoir at moment  $t$  is given as  $Q_\omega(t) = \Phi_\omega S_\omega(t)^{\Psi_\omega}$ .

[76] Combining the continuity and the outflow-storage equations in discrete form and assuming that the input and the output from any reservoir change linearly during the time interval  $\Delta t$ , gives:

$$S_{\omega,n+1} = S_{\omega,n} + \Delta t \left( \tilde{J}_\omega - \Phi_\omega S_{\omega,n+1}^{\Psi_\omega} \right) / 2 \quad (C6a)$$

where

$$\tilde{J}_\omega = E_{\omega,n+1} + E_{\omega,n} + \sum_{k=1}^{\omega-1} p_{k,\omega} \Phi_k \left( S_{k,n+1}^{\Psi_k} + S_{k,n}^{\Psi_k} \right) - \Phi_\omega S_{\omega,n}^{\Psi_\omega} \quad (C6b)$$

for  $\omega > 1$

and

$$\tilde{J}_\omega = E_{\omega,n+1} + E_{\omega,n} - \Phi_\omega S_{\omega,n}^{\Psi_\omega} \quad \text{for } \omega = 1 \quad (C7)$$

[77] Equation (C6) and (C7) are solved iteratively for all storages of order 1 to  $\Omega$  and the output at the outlet of the basin of order  $\Omega$  is  $Q_\Omega(t) = \Phi_\Omega S_\Omega(t)^{\Psi_\Omega}$ .

## C4. Formulation of GNRN in Terms of HG for Basins With Mean Self-Similar Network Topology

[78] All rooted trees contain exactly one stream of the highest-order  $\Omega$  so that  $N_\Omega = 1$ . Therefore incorporating equation (B3) the sequence  $\{N_\omega\}$  and respectively the

Horton's ratio of numbers  $R_B$  is uniquely determined for a binary tree, once the sequence  $\{T_k\}$  has been specified. As a generator of  $\{T_k\}$  we accept Tokunaga's model [Tokunaga, 1966, 1978] which represents a class of trees satisfying the constraints  $T_{\omega, \omega-k} = T_k$  and  $T_{k+1}/T_k = c$  for all  $k$ , where  $c$  is a constant. Such a tree has a generator  $T_k = ac^{k-1}$  and bifurcation ratio given as

$$R_B = \frac{(2+a+c) + \sqrt{(2+a+c)^2 - 8c}}{2} \quad (C8)$$

where  $a$  is a parameter.

[79] Assuming that the Horton's laws of stream numbers  $N_\omega = R_B^{(\Omega-\omega)}$ , lengths  $\bar{L}_\omega = \bar{L}_1 R_L^{(\omega-1)}$  and areas  $\bar{A}_\omega = \bar{A}_1 R_A^{(\omega-1)}$  hold exactly we can rewrite equation (C4) as

$$\Psi_\omega = \frac{\gamma_Q + \delta_Q [\ln \bar{A}_1 + (\omega-1) \ln R_A]}{\gamma_{C_A} + \delta_{C_A} [\ln \bar{A}_1 + (\omega-1) \ln R_A]} \quad (C9a)$$

$$\Phi_\omega = N_\omega F_\omega \quad (C9b)$$

$$F_\omega = \exp\{\alpha_Q + \beta_Q [\ln \bar{A}_1 + (\omega-1) \ln R_A] - \{\alpha_{C_A} + \ln \bar{L}_1 + (\omega-1) \ln R_L + (\Omega-\omega) \ln R_B + \beta_{C_A} [\ln \bar{A}_1 + (\omega-1) \ln R_A]\} \Psi_\omega\} \quad (C9c)$$

[80] According to equation (B3) for a binary tree the number of streams of order  $k$  that drain into streams of order  $\omega$  is given by  $n_{k,\omega} = 2N_\omega + T_{\omega-k}N_\omega$  for  $k = \omega - 1$ , and  $n_{k,\omega} = T_{\omega-k}N_\omega$  otherwise. Since  $p_{k,\omega} = n_{k,\omega}/N_k$  it follows that equation (C6b) can be rewritten as

$$\tilde{J}_\omega = E_\omega^{n+1} + E_\omega^n + \sum_{k=1}^{\omega-1} n_{k,\omega} F_k (S_{k,n+1}^{\Psi_k} + S_{k,n}^{\Psi_k}) - \Phi_\omega S_{\omega,n}^{\Psi_\omega} \quad (C10)$$

[81] Thus both reservoir parameters and the routing procedure can be explained by means of network topology through the generator of  $\{T_k\}$  and Horton's laws' parameters  $R_A$ ,  $R_L$ ,  $\bar{A}_1$  and  $\bar{L}_1$ . Under the above formulation the proposed routing model can be easily modified for different types of tree structures in order to analyze the integral effect of network organization and scale-dependent HG on catchment's hydrologic response.

[82] **Acknowledgments.** This research was supported by the STC program of the National Science Foundation via the National Center for Earth-surface Dynamics (NCED) under agreement EAR-0120914. It was also partially supported by NASA's Land Surface Hydrology Program under grant NAG8-1519. The constructive comments of Vijay Gupta and Murugesu Sivapalan on an earlier draft of this paper resulted in substantial improvement of the presentation of our ideas. Continuous discussions with Gary Parker, Chris Paola and Venugopal Vuruputur have been most inspiring. Computer resources were provided by the Minnesota Super-computing Institute (MSI).

## References

Arad, R. W. (1980), Parameter estimation for symmetric stable distributions, *Int. Econ. Rev.*, *21*, 209–220.  
 Ashmore, P. E., and T. J. Day (1988), Effective discharge for suspended sediment transport in streams of the Saskatchewan River basin, *Water Resour. Res.*, *24*, 864–870.

Bates, B. C. (1990), A statistical log piecewise linear model of at-station hydraulic geometry, *Water Resour. Res.*, *26*, 109–118.  
 Berod, D. D., V. P. Singh, D. Devred, and A. Musy (1995), A geomorphologic nonlinear cascade (GNC) model for estimation of floods from small alpine watersheds, *J. Hydrol.*, *166*, 147–170.  
 Boyd, J. M., D. H. Pilgrim, and I. Cordery (1979), A storage routing model based on catchment geomorphology, *J. Hydrol.*, *42*, 209–230.  
 Carlston, C. W. (1969), Downstream variations in hydraulic geometry of streams: Special emphasis on mean velocity, *Am. J. Sci.*, *267*, 499–509.  
 Dodov, B. A. (2003), Analysis of the effects of channel morphometry and network topology on the nonlinearity of hydrologic response as a function of scale, Ph.D. thesis, Univ. of Minn. Twin Cities, St. Paul.  
 Gupta, V. K., and D. Dawdy (1995), Physical interpretation of regional variations in the scaling exponents in flood quantiles, *Hydrol. Processes*, *9*(3/4), 347–361.  
 Gupta, V. K., and E. C. Waymire (1989), Statistical self-similarity in river networks parameterized by elevation, *Water Resour. Res.*, *25*, 463–476.  
 Gupta, V. K., and E. Waymire (1990), Multiscaling properties of spatial rainfall and river flow distributions, *J. Geophys. Res.*, *95*(D3), 1999–2009.  
 Gupta, V. K., O. J. Mesa, and D. Dawdy (1994), Multiscaling theory of floods: Regional quantile analysis, *Water Resour. Res.*, *30*, 3405–3421.  
 Horton, R. E. (1945), Erosional development of streams and their drainage basins: Hydrophysical approach to quantitative morphology, *Bull. Geol. Soc. Am.*, *56*, 275–370.  
 Huang, H. G., G. C. Nanson, and S. D. Fagan (2002), Hydraulic geometry of straight alluvial channels and the principle of least action, *J. Hydraul. Res.*, *40*(2), 153–160.  
 Lamperti, J. (1966), *Probability: A Survey of Mathematical Theory*, Benjamin, White Plains, N. Y.  
 LeBoutillier, D. W., and P. R. Waylen (1993), A stochastic model of flow duration curves, *Water Resour. Res.*, *29*(10), 3535–3541.  
 Leopold, L. B., and T. Maddock (1953), The hydraulic geometry of stream channels and some physiographic implications, *U.S. Geol. Surv. Prof. Paper*, *252*, 57 pp.  
 Leytham, K. M. (1984), Maximum likelihood estimates for the parameters of mixture distributions, *Water Resour. Res.*, *20*, 896–902.  
 McLachlan, G. J., and T. Krishnan (1997), *The EM Algorithm and Extensions*, John Wiley, Hoboken, N. J.  
 Menabde, M., and M. Sivapalan (2001), Linking space-time variability of rainfall and runoff fields on a river network: A dynamic approach, *Adv. Water Resour.*, *24*(9–10), 1001–1014.  
 Minshall, N. E. (1960), Predicting storm runoff on small experimental watersheds, *J. Hydraul. Div. Am. Soc. Civ. Eng.*, *86*(HYB), 17–38.  
 Park, C. C. (1977), World-wide variations in hydraulic geometry exponents of stream channel: An analysis and some observations, *J. Hydrol.*, *33*, 133–146.  
 Parker, G. (1979), Hydraulic geometry of active gravel rivers, *J. Hydraul. Eng.*, *105*(HY9), 1185–1201.  
 Peckham, S. D. (1995a), Self-similarity in the geometry and dynamics of large river basins, Ph.D. dissertation, Univ. of Colo., Boulder.  
 Peckham, S. D. (1995b), New results for self-similar trees with applications to river networks, *Water Resour. Res.*, *31*, 1023–1029.  
 Pilgrim, D. H. (1976), Travel times and nonlinearity of flood runoff from tracer measurements on a small watershed, *Water Resour. Res.*, *12*, 487–496.  
 Reggiani, P., M. Sivapalan, M. Hassanizadeh, and W. G. Gray (2001), Coupled equations for mass and momentum balance in a stream network: Theoretical derivation and computational experiments, *Proc. R. Soc. London, Ser. A*, *457*, 157–189.  
 Rhoads, B. L. (1991), A continuously varying parameter model of downstream hydraulic geometry, *Water Resour. Res.*, *27*, 1865–1872.  
 Richards, K. S. (1976), Complex width-discharge relations in natural river sections, *Bull. Geol. Soc. Am.*, *87*, 199–206.  
 Rodriguez-Iturbe, I., and A. Rinaldo (1997), *Fractal River Basins*, 547 pp., Cambridge Univ. Press, New York.  
 Rodriguez-Iturbe, I., and J. B. Valdes (1979), The geomorphologic structure of hydrology response, *Water Resour. Res.*, *15*, 1409–1420.  
 Saco, P. M., and P. Kumar (2002a), Kinematic dispersion in stream networks: 1. Coupling hydraulic and network geometry, *Water Resour. Res.*, *38*(11), 1244, doi:10.1029/2001WR000695.  
 Saco, P. M., and P. Kumar (2002b), Kinematic dispersion in stream networks: 2. Scale issues and self-similar network organization, *Water Resour. Res.*, *38*(11), 1245, doi:10.1029/2001WR000694.

- Schertzer, D., and S. Lovejoy (1987), Physical modeling and analysis of rain and clouds by anisotropic scaling multiplicative processes, *J. Geophys. Res.*, 92(D8), 9693–9714.
- Schumm, S. A. (1956), Evolution of drainage systems and slopes in badlands at Perth Amboy, New Jersey, *Geol. Soc. Am. Bull.*, 67, 597–646.
- Singh, K. P., and R. A. Sinclair (1972), Two distribution method for flood frequency analysis, *J. Hydraul. Div. Am. Soc. Civ. Eng.*, 98(HY1), 29–42.
- Smith, J. A. (1992), Representation of basin scale in flood peak distributions, *Water Resour. Res.*, 28, 993–2999.
- Sposito, G., and W. A. Jury (1988), The lifetime probability density function for solute movement in the subsurface zone, *J. Hydrol.*, 102, 503–518.
- Stall, J. B., and Y. S. Fok (1968), Hydraulic geometry of Illinois streams, *Ill. Water Resour. Res. Rep.*, 15, 47 pp.
- Strahler, A. N. (1952), Hypsometric (area-altitude) analysis of erosional topography, *Geol. Soc. Am. Bull.*, 64, 165–176.
- Strahler, A. N. (1957), Quantitative analysis of watershed geomorphology, *Eos Trans. AGU*, 38(6), 913–920.
- Tokunaga, E. (1966), The composition of drainage network in Toyohira River Basin and the valuation of Horton's first law, *Geophys. Bull. Hokkaido Univ.*, 15, 1–19.
- Tokunaga, E. (1978), Consideration on the composition of drainage networks and their evolution, *Geogr. Rep.* 13, 27 pp., Tokyo Metrop. Univ., Tokyo.
- Wang, C. T., V. K. Gupta, and E. Waymire (1981), A geomorphologic synthesis of nonlinearity in surface runoff, *Water Resour. Res.*, 17, 545–554.
- Wong, T. H. F., and E. M. Laurenson (1984), A model of flood wave speed-discharge characteristics in rivers, *Water Resour. Res.*, 20, 1883–1890.

---

B. Dodov and E. Foufoula-Georgiou, St. Anthony Falls Laboratory, Department of Civil Engineering, and National Center for Earth-surface Dynamics, University of Minnesota Twin Cities, Mississippi River at 3rd Ave. SE, Minneapolis, MN 55414, USA. (efi@tc.umn.edu)